Organisation for Economic Co-operation and Development

ENV/CBC/MONO(2022)27/ANN1

Unclassified

English - Or. English

3 September 2022

ENVIRONMENT DIRECTORATE
CHEMICALS AND BIOTECHNOLOGY COMMITTEE

ANNEX I. PHYSIOLOGICALLY BASED PHARMACOKINETIC MODELLING OF ACETAMIPRID, IMIDACLOPRID AND DESNITROIMIDACLOPRID within Case Study on the use of Integrated Approaches for Testing and Assessment for developmental neurotoxicity hazard characterisation of acetamiprid

Series on Testing and Assessment
No. 365

JT03501785

OECD Environment, Health and Safety Publications

SERIES ON TESTING AND ASSESSMENT

NO. 365

ANNEX I. PHYSIOLOGICALLY BASED PHARMACOKINETIC MODELLING OF ACETAMIPRID, IMIDACLOPRID AND DESNITROIMIDACLOPRID within Case Study on the use of Integrated Approaches for Testing and Assessment for developmental neurotoxicity hazard characterisation of acetamiprid

IOMC

INTER-ORGANIZATION PROGRAMME FOR THE SOUND MANAGEMENT OF CHEMICALS

A cooperative agreement among FAO, ILO, UNDP, UNEP, UNIDO, UNITAR, WHO, World Bank and OECD

Environment Directorate

ORGANISATION FOR ECONOMIC COOPERATION AND DEVELOPMENT

Paris 2022

About the OECD

The Organisation for Economic Co-operation and Development (OECD) is an intergovernmental organisation in which representatives of 38 industrialised countries in North and South America, Europe and the Asia and Pacific region, as well as the European Commission, meet to co-ordinate and harmonise policies, discuss issues of mutual concern, and work together to respond to international problems. Most of the OECD's work is carried out by more than 200 specialised committees and working groups composed of member country delegates. Observers from several countries with special status at the OECD, and from interested international organisations, attend many of the OECD's workshops and other meetings. Committees and working groups are served by the OECD Secretariat, located in Paris, France, which is organised into directorates and divisions.

The Environment, Health and Safety Division publishes free-of-charge documents in twelve different series: **Testing and Assessment**; **Good Laboratory Practice and Compliance Monitoring**; **Pesticides**; **Biocides**; **Risk Management**; **Harmonisation of Regulatory Oversight in Biotechnology**; **Safety of Novel Foods and Feeds; Chemical Accidents; Pollutant Release and Transfer Registers; Emission Scenario Documents; Safety of Manufactured Nanomaterials;** and **Adverse Outcome Pathways.** More information about the Environment, Health and Safety Programme and EHS publications is available on the OECD's World Wide Web site (www.oecd.org/chemicalsafety/).

This publication was developed in the IOMC context. The contents do not necessarily reflect the views or stated policies of individual IOMC Participating Organizations.

The Inter-Organisation Programme for the Sound Management of Chemicals (IOMC) was established in 1995 following recommendations made by the 1992 UN Conference on Environment and Development to strengthen co-operation and increase international co-ordination in the field of chemical safety. The Participating Organisations are FAO, ILO, UNDP, UNEP, UNIDO, UNITAR, WHO, World Bank and OECD. The purpose of the IOMC is to promote co-ordination of the policies and activities pursued by the Participating Organisations, jointly or separately, to achieve the sound management of chemicals in relation to human health and the environment.

This publication is available electronically, at no charge.

- **Also published in the Series on Testing and Assessment: link**

For this and many other Environment, Health and Safety publications, consult the OECD's World Wide Web site (www.oecd.org/chemicalsafety/)

or contact:

OECD Environment Directorate,
Environment, Health and Safety Division
2 rue André-Pascal
75775 Paris Cedex 16
France

E-mail: ehscont@oecd.org

Report objective

To provide a description of methods and relevant equations for the physiologically based pharmacokinetic (PBPK) models constructed for Acetamiprid, Imidacloprid and Desnitroimidacloprid within the framework of the EU_TOX_RISK project. The main use of the PBPK models is to assess the plasma and brain concentrations following ingestion of single or multiple doses of the compounds. This information is being used within the context of an IATA considering the developmental neurotoxicity (DNT) potential of the compounds.

In this context of use a PBPK model is not intended to precisely characterise the PK processes but to represent an interpretation of the available data by addressing the relationships between an external dose and internal tissue, blood or excretion dose (WHO publication Harmonization Project Document No. 9. CHARACTERIZATION AND APPLICATION OF PHYSIOLOGICALLY BASED PHARMACOKINETIC MODELS IN RISK ASSESSMENT).

In constructing the PBPK models for imidacloprid, desnitroimidacloprid and acetamiprid the following aspects were considered as suggested in the WHO PBPK guidance.

1) The critical effect caused by the chemicals was DNT.
2) Parent compound was assumed to be the toxic moiety
3) The physiology (i.e. tissue weights and blood flow rates) of the species of interest were the default values in the Simcyp rat and human simulator (V19 or V20).

Specific aims of the modelling exercise were

1) To develop PBPK models to predict comparative human exposure of the compounds using *in vitro* to *in vivo* extrapolation approaches
2) To examine the inter-individual variability in the simulated exposure of the compounds in humans.

PBPK model assumptions

The following assumptions have been made in the development of PBPK models for acetamiprid, imidacloprid and desnitroimidacloprid:

1) The metabolism of the compounds is assumed to be linear (i.e. not to saturate) over the range of doses simulated.
2) For acetamiprid and imidacloprid the pharmacokinetics of the parent compound was assumed to be represented by the deuterated compounds used in the human oral study for the compounds described by Harada *et al*. (2016)

Table of contents

FIGURES

TABLES

ABBREVIATIONS

AAG	alpha-1 acid glycoprotein
ADAM	advanced dissolution, absorption and metabolism model
ADME	absorption, metabolism, distribution and excretion
AUC	area under the plasma drug concentration-time curve
BCRP	breast cancer resistance protein
BSA	body surface area
B/P	ratio of concentration of drug in blood to plasma
C_{max}	maximum plasma concentration
C_{ss}	plasma drug concentration at steady state
CL_{int}	intrinsic metabolic clearance
CLu_{int}	unbound intrinsic metabolic clearance
CL	intravenous clearance
CL_R	renal clearance
CV	coefficient of variation
CYP	cytochrome P450
E_G	gut extraction ratio
E_H	hepatic extraction ratio
E:P	erythrocyte : plasma ratio
fa	fraction absorbed
fm	fraction metabolised
fu	fraction unbound in plasma
fu_{EW}	unbound fraction in the extracellular water
fu_{IW}	unbound fraction in the intracellular water
fu_{mic}	fraction of unbound substrate or inhibitor in a microsomal incubation
GI	gastrointestinal tract
HC	haematocrit
HBD	number of hydrogen bond donors
HPGL	hepatocellularity per gram of liver
HV	healthy volunteer
HLM	human liver microsomes
HSA	human serum albumin
IVIVE	*in vitro in vivo* extrapolation
J_{max}	maximum rate of transporter mediated uptake or efflux
k_a	absorption rate constant
K_m	Michaelis constant
logP	log octanol/buffer partition coefficient (neutral species)
MPPGL	microsomal protein per gram of liver

MSR	maximum supersaturation ratio
NEC	North European Caucasian
Papp	apparent *in vitro* permeability
$P_{eff,man}$	*in vivo* effective permeability in humans
P-gp	Permeability-limiting glycoprotein, encoded by the multidrug resistance 1 (MDR1) gene
PBPK	physiologically based pharmacokinetic
PK	pharmacokinetic(s)
pK_a	acid dissociation constant
PRC	precipitation rate constant
PSA	polar surface area
$P_{Tissue:p}$	partition coefficient of drug between tissues and plasma
Q_H	hepatic blood flow
QSPR	Quantitative Structure-Property Relationship
RAF/REF	relative activity or expression factor
rhCYP	recombinantly expressed human CYP enzyme
t_{max}	time at which the maximum plasma concentration of drug is reached
V_{max}	maximum metabolic rate
V_C	volume of central compartment
V_{ss}	volume of distribution at steady state

Introduction

PBPK models were constructed for acetamiprid, imidacloprid and desnitroimidacloprid.

Acetamiprid is a neutral compound with a reported Log P_{ow} of 0.8 (1: Brunet et al, 2008). Acetamiprid has high permeability across the Caco-2 cell monolayer with an apparent permeability (Papp) value of 26 x 10^{-6} cm/s reported (1: Brunet et al, 2008).

There have been relatively few studies that have studied the *in vivo* pharmacokinetics of acetamaprid. Ford and Casida have studied the metabolism and tissue distribution of acetamiprid following intraperitoneal injection in mice (2: Ford et al, 2006). Metabolites identified included the desmethyl metabolite and various cleavage products. Both parent compound and the desmethyl metabolite were detected in the brain, liver, plasma and urine of the mice. The levels of parent compound in the brain were about half of those in the plasma at equivalent time points. Other studies have also measured brain concentrations of acetamiprid after exposure via drinking water to mice (3: Terayama et al, 2016). Unfortunately in this study plasma concentrations were not reported to allow a brain:plasma ratio to be calculated.

Studies with radiolabelled acetamiprid in rats show rapid and extensive absorption of radioactivity after single (1 or 50 mg/kg) or multiple (1 mg/kg) doses. With rapid excretion of radioactivity mainly via the urine. In both rats and goats demethylation of acetamiprid is a major metabolic pathway (EFSA opinion).

In humans the urinary excretion of deuterated acetamiprid and desmethylacetamiprid following oral dosing of deuterated (D6) acetamiprid (5 mg) has been measured (4: Harada et al, 2016). The urinary excretion of acetamiprid (2.6% of the dose) was lower than that of the desmethyl metabolite (31% of the dose). In an additional part of the study by Harada *et al*. (2016) desmethylacetamiprid was found in the urine of every subject (n=373) where measurement was attempted. Using a pharmacokinetic model it was estimated that for a daily intake of 1.94 mg/d of acetamiprid a total of 1.14 mg/d would be excreted in the urine as desmethylacetamiprid (~63% of the dose once differences in molecular weight are accounted for).

Imidacloprid is a neutral compound with a reported Log P_{ow} of 0.57 (Pubchem). There have been relatively few studies that have studied the *in vivo* pharmacokinetics of imidacloprid although data for total radioactivity following dosing of ^{14}C-imidacloprid are available. Following dosing of 20mg/kg imidacloprid in corn oil to female rats the oral blood clearance of imidacloprid was 3.4 ml/min/kg (5: Kapoor et al, 2014). Based on the reported AUC in blood and brain (5: Kapoor et al, 2014) the tissue:blood ratio in female rats was calculated to be 0.47. In mice the brain:plasma ratio has been reported to be ~ 0.75 (2: Ford et al, 2006).

In vivo in the rat imidacloprid is extensively metabolised. In the literature metabolism of imidacloprid by both aldehyde oxidase and cytochromes P450 have been reported (2: Ford et al, 2006, 6-10: Wang et al, 2018). The different routes of metabolism of imidacloprid have been summarised in the review by Wang et al., (10: Wang et al, 2018). CYP isozymes including CYP3A4, 2C19,2A6 and2C9 were shown to form 5-hydroxy imidacloprid and lower amounts of the olefin and desnitro metabolite (8: Schulz-Jander and Casida, 2002, 9: Schulz-Jander et al, 2002). Other reports show the formation of more potent metabolites of imidacloprid by aldehyde oxidase with little increase in potency was seen when imidacloprid was incubated with CYP 3A4 (11: Honda et al, 2006). Other studies have shown that aldehyde oxidase reduces imidacloprid but detected an aminoguanidine product rather than a guanidine (desnitro) metabolite (6: Dick et al, 2005).

In the *in vitro* metabolism studies conducted in human hepatocytes for the EU_TOX-Risk project although metabolism of parent imidacloprid was too slow to accurately quantify the disappearance of imidacloprid (see below for further information) and calculate an *in vitro* intrinsic clearance, formation of some metabolites of imidacloprid were observed in human hepatocytes. However, the only metabolites observed were the 5-OH and olefin metabolites which are thought to be formed by CYP isozymes. This is despite the cells showing the capability to metabolise known aldehyde oxidase substrates such as carbazeran(12: Dalvie et al, 2019). Further studies to characterize the metabolism of imidacloprid with the aim of being to able to determine the rate and extent of the metabolism of imidacloprid to the desnitro metabolite are ongoing.

Separate PBK models were developed for Imidacloprid and desnitroimidacloprid as the desnitro metabolite is also present in crops that have been treated with imidacloprid. The two models can be linked together if information on the rate and extent of desnitroimidacloprid formation from imidacloprid becomes available.

Methods and Model Development

PBPK models were constructed in the rat and human Simcyp Simulator (V19 or V20 for desnitroimidacloprid) (www.simcyp.com). The Simcyp simulator has been extensively tested and used by a consortium of industry, regulatory and academic scientists. Lists of known bugs within the code of the Simcyp simulator are maintained on our website (https://members.simcyp.com/account/softwareIssues/). The QA system used to support the production of each version of the Simcyp simulator has been described in detail (13: Jamei et al, 2013).

2.1.1 Physiologically based pharmacokinetic models

An aim of the PBPK modelling study was to estimate the concentrations of compounds in different tissues of the body including the brain which is the target organ for toxicity of these agents in the AOP under investigation. To accomplish this a full body physiologically based pharmacokinetic (PBPK) model (Figure 1) was used. In the human simulator the ability to add further specific organs as an additional organ is available, but in the simulations for Acetamiprid, Imidacloprid and Desnitroimidacloprid this functionality was not used.

Figure 1. A physiologically based pharmacokinetic model.
Q_H, $Q_{H,A}$, Q_{PV}, Q_G, $Q_{T,A}$ and Q_T are blood flows in the hepatic vein, hepatic artery, hepatic portal vein, gut and blood flows into and out of the other tissue (T) compartments, respectively; E_G and E_H are the fractions undergoing first pass metabolism in the gut and liver, respectively; CL_R is the renal clearance; fa and ka are the fraction absorbed and the first order absorption rate constant, respectively.

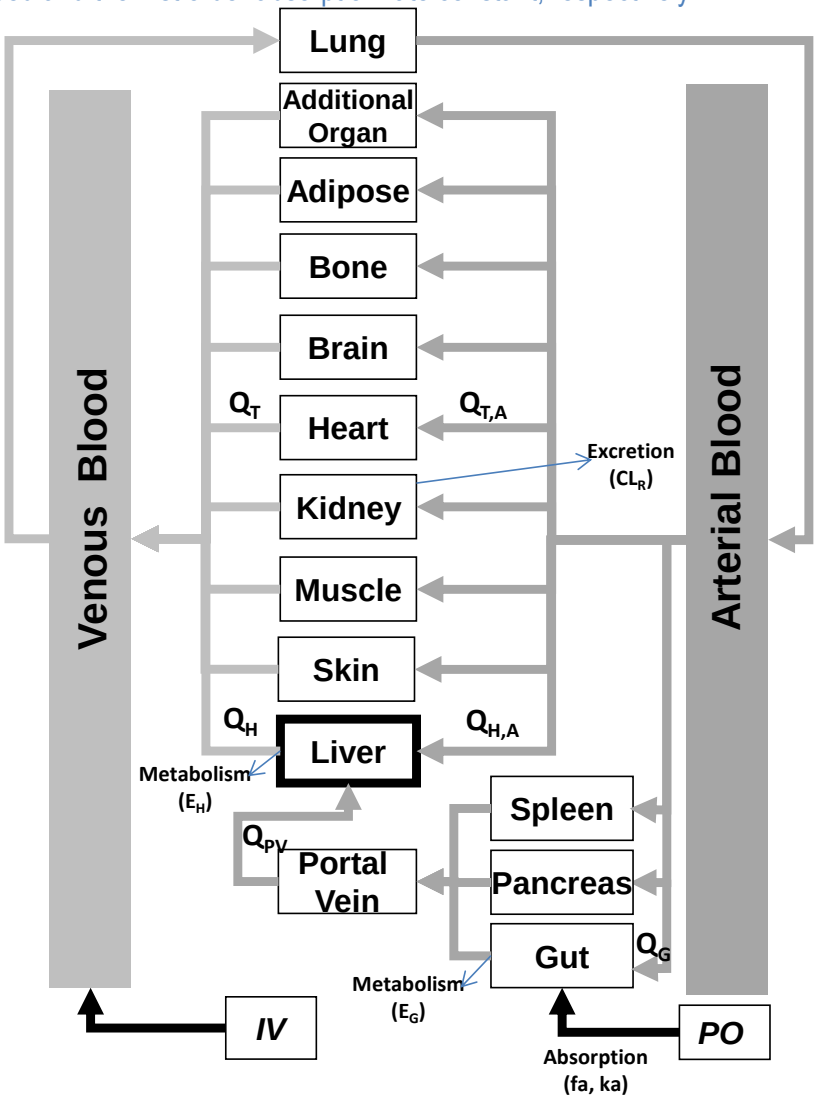

Distribution

In the human simulator inter-individual variability in tissue distribution is accounted for through relationships between tissue volume and age, sex, weight and height (14: Jamei et al, 2009). In both the human and rat PBPK models the *in vivo* volume of distribution at steady state (V_{ss}) is predicted using Equation 1 from Sawada *et al.* (15: Sawada et al, 1984):

$$V_{ss} = (\sum V_T \times P_{T:p}) + (V_e \times E:P) + V_p \qquad \text{Equation 1}$$

Where V is the fractional body volume (L/kg) of a tissue (T), erythrocytes (e), and plasma (p), E:P is the erythrocyte:plasma drug concentration ratio and PT:p is the partition coefficient of drug between tissues

and plasma components. Three methods are available for prediction of PT:p. The first method was reported by Poulin and Thiel (16: Poulin and Theil, 2002) as corrected by Berezhkovskiy (17: Berezhkovskiy, 2004) (Method 1). Method 1 uses the physicochemical properties of the compounds (pKa and log P) together with in vitro information (B/P and fu) to predict partitioning into the tissues with the assumption that tissues and plasma are mixtures of lipids, water and proteins with a global pH of 7.4.

The second method was developed by Rodgers and Rowland (18: Rodgers and Rowland, 2006) (Method 2). The latter splits the tissue water volume into intra- and extracellular components, along with the addition of a tissue acidic phospholipid fraction. These equations take explicit account of the extent of ionisation of a compound at the pH of the compartment concerned and have been shown to improve the prediction of tissue:plasma partition coefficients, and consequently Vss, for strong bases. The Rodgers and Rowland method was further extended by the science team at Simcyp to account for the effect of differences in membrane potential in the different tissues on compound distribution (Method 3). Method 3 is only available in the human PBPK models and also allows for the distribution of compounds into specific subcellular organelles to be modelled. Method 3 also forms the basis for the biokinetic model developed within the EU-TOX-Risk project (19: Fisher et al, 2017). These mechanistic predictions assume non-saturating conditions prevail for all binding processes, drug transport is via passive processes (i.e. no active transport), and each tissue has a well-stirred distribution limited by blood perfusion (i.e. perfusion limited not permeability limited).

Performance verification for both Method 1 and Method 2 in the rat with a wide range of compounds (molecular weight of 192-1202kDa, 19% acidic, 46% basic, 9% neutral, 27% ampholyte) is shown in Figure 2. The range of *in vivo* Vss for the studied compounds was 0.17-19.9 L/kg and for Method 1 and Method 2, 64% and 82% of predictions were within 2-fold of observed values, respectively.

Figure 2. Performance verification of Vss predictions in Rat for Method 1 (P&T, blue diamonds) and Method 2 (R&R, purple triangles)

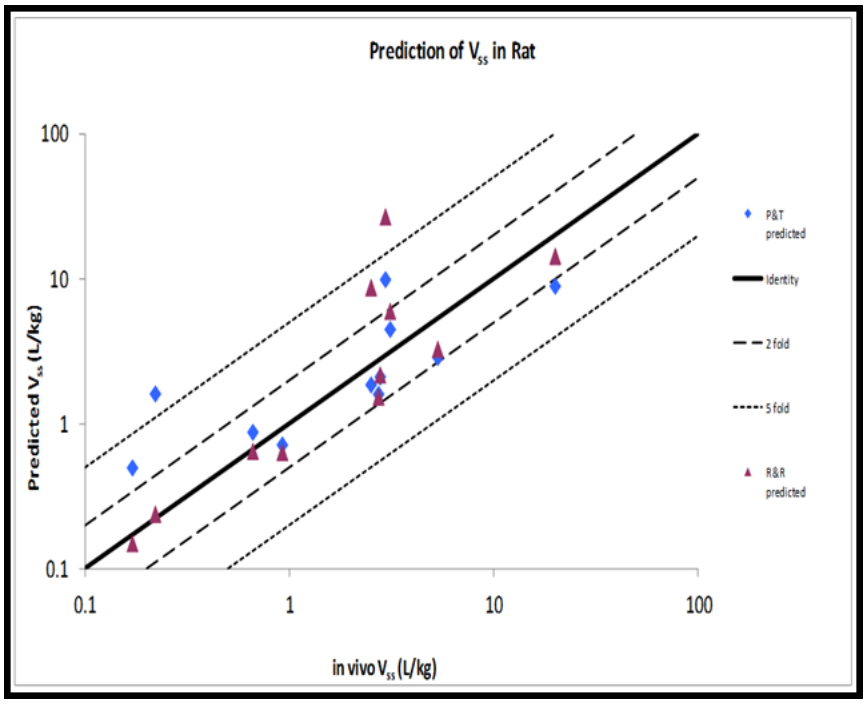

Perfusion and permeability limited distribution

Lipophilic drugs diffuse rapidly across the capillary membrane into tissue interstitial fluid such that blood flow to the tissue is the rate-limiting step in uptake. This is described as perfusion-limited distribution and is implemented in all tissues represented in the PBPK model (Figure 1). In addition, an option is provided within the Simcyp Simulator to allow for permeability-limited uptake, simulating both passive diffusion in parallel with active uptake and efflux in specific organs such as the liver, kidney (human only), intestine and brain. In these models the tissue is divided into compartments representing vascular, extracellular and intracellular fluid spaces - with distribution between these spaces defined as a dynamic process. The 'permeability-limited' models in the liver, brain and kidney are only available when Method 2 or 3 are selected to predict $P_{T:p}$. Given the moderately lipophilic nature of acetamiprid and imidacloprid perfusion limited models were used for all tissues in the simulations presented here.

Oral Absorption

For drugs in solution, several absorption models are available within the Simcyp Simulator including a first-order absorption model and the advanced dissolution absorption metabolism (ADAM) model (20: Jamei et al, 2009). Simulation of the absorption of drugs from solid dosage forms requires use of the ADAM model. The ADAM model, as implemented in the Simcyp Simulator, divides the gastro-intestinal tract (GIT) into nine anatomically defined segments from the stomach through the intestine to the colon (Figure 3). Drug absorption from each segment is described as a function of release from the formulation, dissolution, precipitation, luminal degradation, permeability, metabolism, transport and transit from one segment to another. It is assumed that absorption from the stomach is insignificant compared with that from the small intestine, and that movement of liquid and solid drug through each segment of the GIT may be described by first-order kinetics. Dissolution rate from solid dosage forms is calculated from information on drug aqueous solubility and particle size using diffusion layer models (DLM) (21: Wang and Flanagan, 1999, 22: Wang and Flanagan, 2002).

Figure 3. (A): Structure of the ADAM model in which the GI tract is divided into 9 sections with segregated blood flows to each section.
The abundance of various enzymes and transporters in each segment varies non-monotonically along the intestine as indicated by the varying intensity of the colour for each section (BCRP distribution is indicated) (23: Harwood et al, 2013, 24: Harwood et al, 2016).

(B): Segment of the small intestine indicating the various processes that can be simulated (from (25: Darwich et al, 2010).

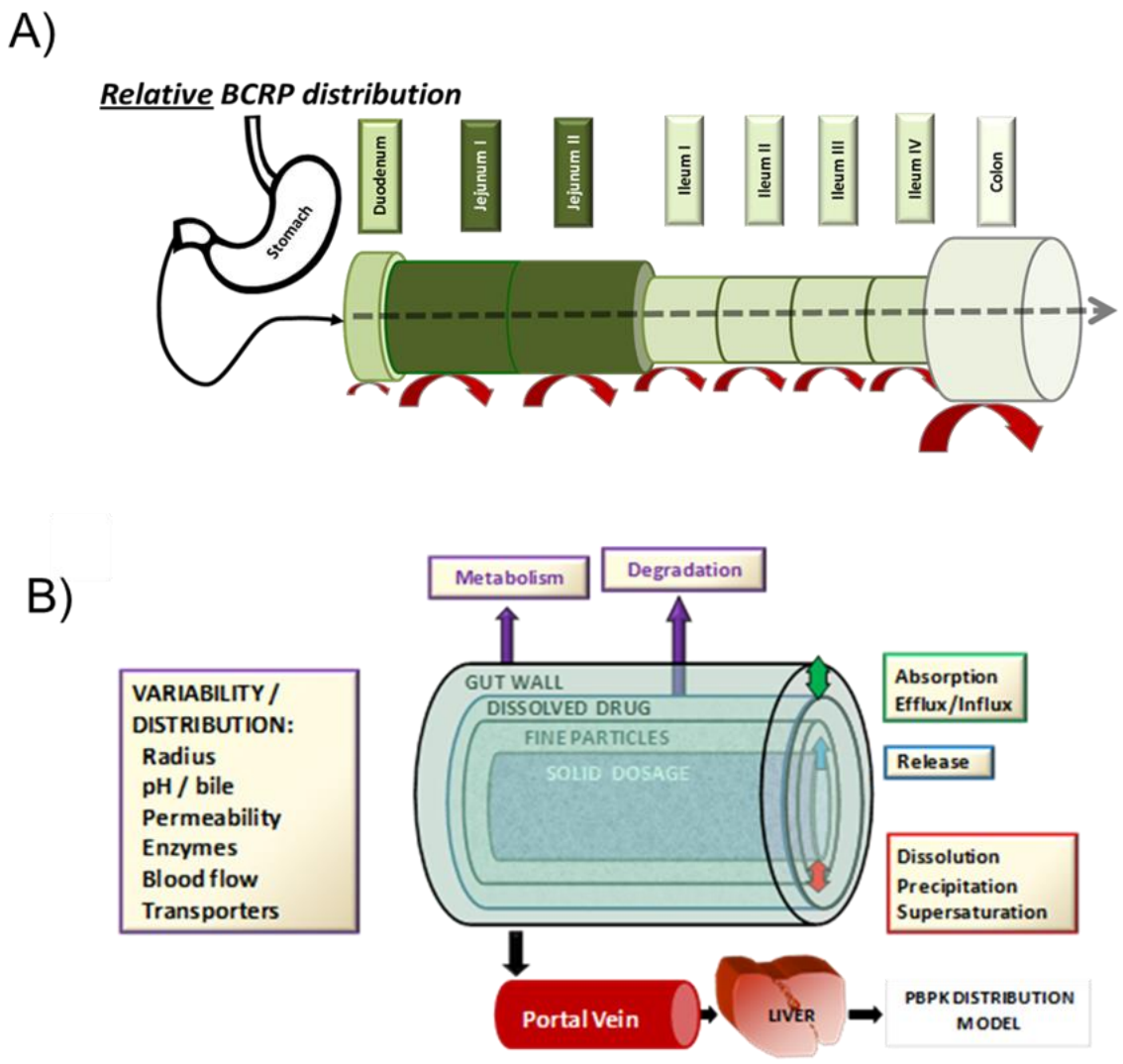

The effective permeability in humans, Peff,man (jejunal), can be measured using the Loc-i-gut methodology and can be used in simulations to describe the absorptive processes in the intestine (26: Nilsson et al, 1994). For novel investigational drugs and many marketed agents and all industrial chemicals measured values of Peff,man (jejunal) are not available and therefore several methods can be used within the Simcyp Simulator to predict Peff,man (jejunal). These are based on data obtained with cell lines (such as Caco-2, MDCK-II or LLC-PK1 cells)(27: Sun ea al, 2002), PAMPA or from a QSPR model based upon physicochemical properties (PSA and HBD,(28: Winiwarter ea al, 1998)) or by using the mechanistic permeability (MechPeff) model (Figure 4). The regional permeability (seven small intestine segments plus

colon) is assumed to be the same by default but can be modified by the user. The regional distributions of drug metabolising enzymes and efflux transporters such as P-gp and BCRP are also incorporated, allowing simulation of the effects of efflux transport and metabolism on drug absorption (Figure 3A).

Figure 4. Input options to predict P_{eff} and subsequently absorption within the Simcyp Simulator. The physicochemical based QSPR (HBD and PSA) and MechPeff models were used in the simulations in this study.

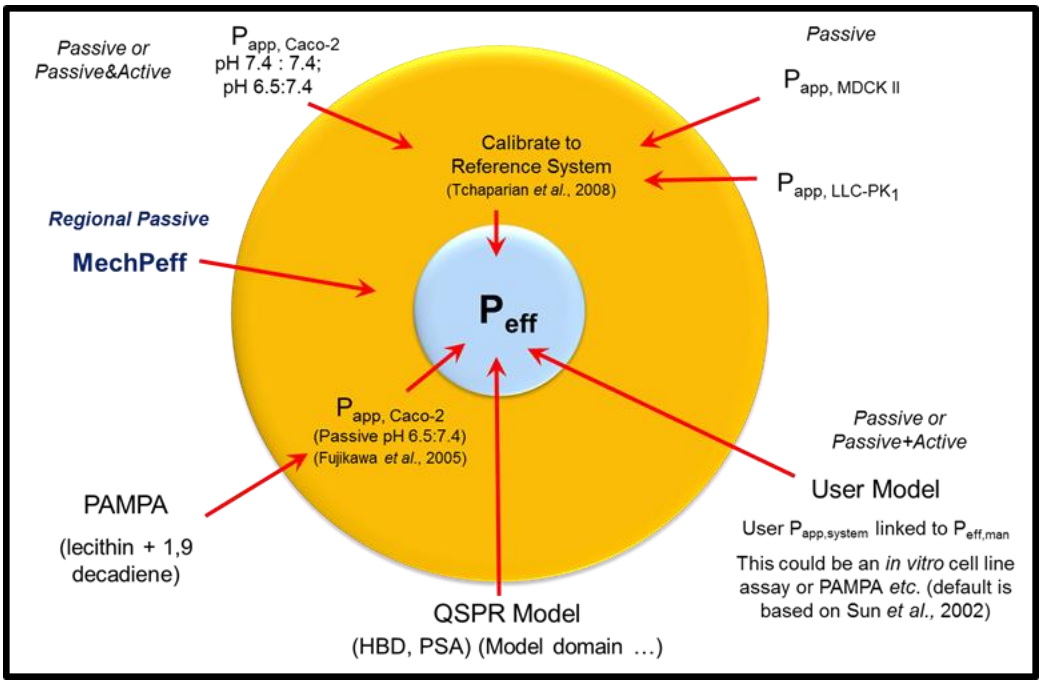

The MechPeff Model is a fully mechanistic model that predicts passive intestinal permeability using a compound's physicochemical parameters such as LogP, pKa, molecular weight and compound type. The MechPeff model within Simcyp is adapted from the original structure described by Sugano (29: Sugano, 2009). In brief, the model considers:

1) Intrinsic transcellular permeability according to the pH-partition hypothesis (default setting) but allows the user to select an additional model permitting transcellular ion permeation if desired;
2) Paracellular permeability based on the chemical's molecular size in relation to paracellular pore sizes (modelled via a Renkin function). In addition pore charge-charge interactions are considered (ionic species as well as neutral species can pass through the paracellular pathways)
3) The luminal Unstirred Boundary Layer (UBL) which may be the rate limiting barrier for otherwise highly permeable compounds.

A scaling procedure is used to account for the impact of the varying regional GI morphology and physiology along the rat small intestine upon P_{eff}. A further scaling of effective available absorptive surface area, according to epithelial permeability, is provided. This accounts for the fact that highly permeable compounds may be almost entirely absorbed at the villi tips while less permeable compounds will tend to diffuse down the inter-villus spaces and thus be exposed to a larger effective surface area. This scaling procedure is based upon the model described by Oliver *et al*. (30: Oliver et al, 1998). The model also considers the impact of partitioning of the compound into bile salt micelles upon P_{eff}.

2.1.1.3.1 Supersaturation and Precipitation

Supersaturation describes the phenomenon whereby in the intestine some chemicals can remain in solution at concentrations above their thermodynamic equilibrium solubility and can be particularly important for poorly soluble compounds. Supersaturation is often observed for ionised compounds when there are abrupt pH changes. For example the pH change when moving from the stomach (pH 1.5-3.5) to the duodenum (pH 5-7) can promote precipitation of weakly basic compounds, (pKa values 5 to 8)(31: Hsieh et al, 2012). Dependent on the rate of precipitation of the chemical and the relative solubilities of the ionised and unionised forms of the chemical this can lead to a supersaturated solution being formed (31: Hsieh et al, 2012)(Figure 5). When compounds can supersaturate, the maximal extent and duration of supersaturation is very much compound-dependent and whilst this can be measured experimentally (31: Hsieh et al, 2012), it cannot currently be (accurately and consistently) predicted.

Figure 5. Schematic of supersaturation phenomenon for a weakly basic drug which is soluble at low pH (e.g. stomach) and subsequent formation of the less soluble species at higher pH (e.g. intestine).

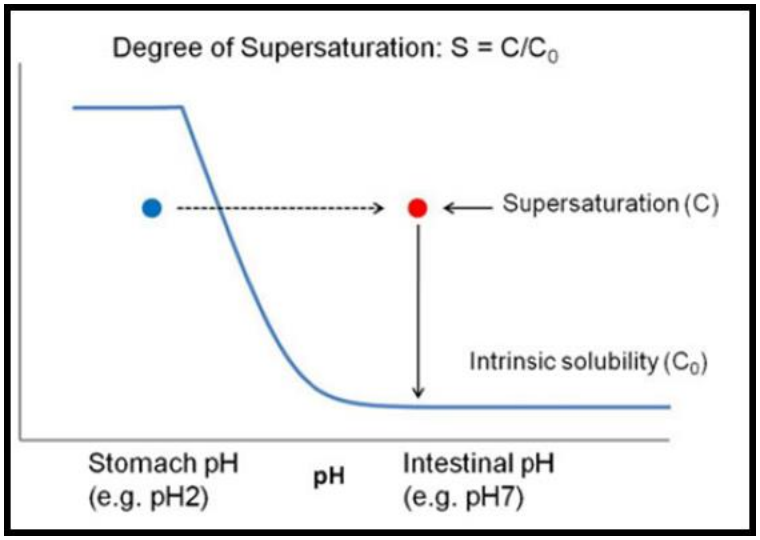

Within Simcyp the extent and duration of supersaturation is specified by two parameters the maximum supersaturation ratio (MSR) and a first order precipitation rate constant (PRC). The MSR specifies the maximal allowable extent of supersaturation of a compound in solution in the gut lumen defining the maximum ratio of kinetic solubility to equilibrium solubility. When luminal compound concentrations exceed this maximum kinetic solubility (MKS) precipitation occurs. When the concentration is reduced to (or below) the MKS the precipitation rate is defined by a first order rate constant (PRC). Precipitation no longer occurs once the luminal drug concentration is equal to, or less than, the equilibrium solubility (32: Brouwers et al, 2009).

The PRC is applied to total dissolved compound concentration including that in the ionised state and compound partitioned into bile micelles. Thus it is assumed that the inter-conversion of the compound between neutral and ionised states and the partition/departition of these monomers into bile micelles are not rate limiting for precipitation. For a given pH and bile salt concentration it is assumed that the proportions of compound in the neutral, ionised and bound (within micelles) states are constant. The default PRC of 4 h^{-1} is equivalent to a mean duration of 15 minutes for the supersaturated state thus increasing the time available for the dissolved compound to be absorbed.

Metabolic Clearance

Elimination of a compound can be characterized by various inputs of clearance such as intravenous or oral clearance (CL_{iv} or CL_{po}), whole organ metabolic clearance via hepatocytes (CL_{int}; µL/min/10^6 cells), liver and intestinal microsomes (CL_{int}; µL/min/mg) or incubation with intestinal slices (CL_{int}; µL/min/g of intestine).

2.1.1.4.1 Hepatic metabolic clearance

On a general basis the *in vivo* hepatic metabolic clearance is predicted using *in vitro-in vivo* extrapolation (IVIVE) as shown schematically in

Figure 6 followed by scaling for the specific metabolising tissue blood flow (liver in this case) and fraction of unbound drug in blood.

Figure 6. Schematic of IVIVE for scaling of *in vitro* intrinsic clearance available for the Simcyp Simcyp simulator.

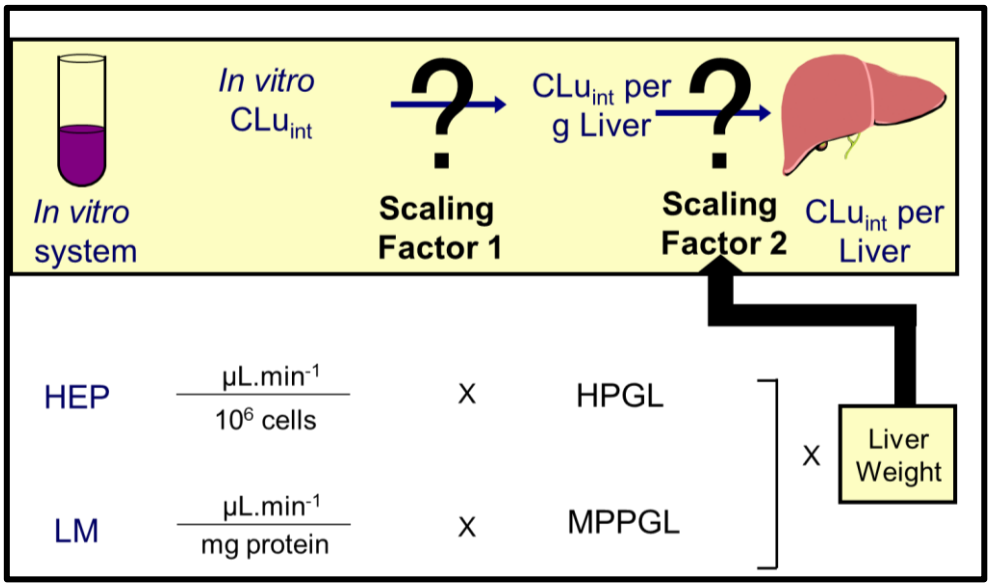

For the human simulator clearance PBPK models clearance can be predicted using metabolic intrinsic clearance (Clint, hep) data generated in cryopreserved human hepatocytes or other in vitro experimental systems. In vitro $CL_{int,hep}$ was scaled up to the in vivo Clint ($Clint_{u,H}$) according to **Equation** .

$$CLint_{u,H} = \frac{CLint,hep}{fu,hep} \times Uptake \times HPGL\ Scaling\ Factor \times Liver\ Weight \times 10^{-6}\ x\ 60$$

Equation 4

Where fu_{hep} is the fraction unbound of the compound in the hepatoycte incubation, HPGL is the number of hepatocytes per gram of liver, uptake was assumed to be only due to passive processes in these simulations (set =1), and 10^{-6} and 60 are to adjust units from µl/min per 10^6 cells to L/h in the whole liver.

Correction for non-specific protein binding is important for IVIVE (33: Brown et al, 2007, 34: McGinnity et al, 2006). Fu,hep was predicted from an estimate of the fraction unbound in microsomal incubations

(fu,mic) as described by Kilford et al (35: Kilford et al, 2008). Fu,mic may be determined experimentally by equilibrium dialysis, ultrafiltration or ultracentrifugation methods (36: Giuliano et al, 2005). Measured values of fumic were not available for the compounds studied in this exercise, and therefore in order to account for non-specific binding of the compound in the incubation, fumic was predicted using the QSAR model implemented within the Prediction toolbox in the Simcyp Simulator (V19). The Simcyp fumic prediction is based on a dataset of both human and rat liver microsomes. It has been shown that there are no species differences in microsomal binding once corrections for any differences in protein content in the incubation are accounted for (37: Zhang et al, 2010). The fumic prediction model with Simcyp uses separate models for fully ionised acids, bases and neutral compounds (38: Turner et al, 2006). The fumic for a partially ionised compound is calculated as described by Gao et al. (39: Gao et al, 2010).

$$fu_{hep} = \frac{1}{1 + \frac{K_{HM}}{K_{mic}} \times \frac{V_R}{P} \times \left(\frac{1 - fu_{mic}}{fu_{mic}}\right)}$$ Equation 5

Where Kmic represents microsomal protein binding affinity, P the microsomal protein concentration (mg/ml), KHM the hepatocyte/medium concentration ratio, and VR a Vcell/Vinc ratio, where Vcell is the cell volume and Vinc the incubation volume. A KHM/Kmic ratio of 125 was assumed (35: Kilford et al, 2008). VR is 0.005 at the cell concentration of 106 cells/ml (35: Kilford et al, 2008), and was normalised for P of 1 mg/ml.

The hepatic clearance (CL_H) in humans was calculated from the whole liver scaled *in vivo* Clintu using the well stirred model (equation 6).

$$CL_H = \frac{Q_H * Clint_{u,h} * fu_B}{Q_H + (Clint_{u,h} * fu_B)}$$ Equation 6

Where Q_H = hepatic blood flow, $Clint_{u,h}$ is the *in vivo* hepatic intrinsic clearance and fu_B = fu/(B/P).

The accuracy of this in vitro – in vivo approach to predict human clearance from human hepatocytes using data generated in human hepatocytes under the same experimental method as used for acetamiprid, imidacloprid and desnitroimidacloprid is shown below (Figure 7). The range of LogP values for these compounds was -0.07 to 4.8 although the highest log P for a neutral compound was 2.82.

Figure 7. Relationship between predicted and observed human Clearance for a series of 18 compounds.

The predicted clearance was made using IVIVE approaches based on in vitro intrinsic clearance generated in human hepatocytes by Cyprotex.

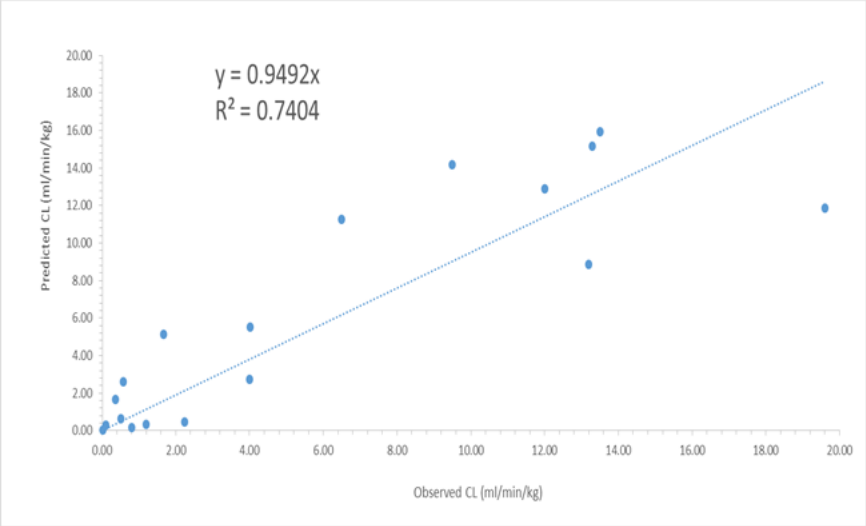

2.1.1.4.2 Metabolic Clearance in Children

As well as differences in body and tissue sizes that will affect the capacity of children to clear chemicals the different enzyme systems involved in drug metabolism mature at different rates with some having the same amount of enzyme (per mg microsomal protein) as adults whereas other enzymes have much lower levels of enzymes (per mg microsomal protein) at birth and reach adult levels with different trajectories. Within the Simcyp simulator the maturation of different enzymes is described by ontogeny functions. For Imidacloprid simulations were conducted in young children (0.24 – 0.26 years old) as well as Adults. In the *in vitro* experiments we conducted we were not able to definitively define the enzymes involved in imidacloprid metabolism to allow the ontogeny profiles of individual enzymes to be considered. To account for possible differences in the maturation of the enzymes involved in imidacloprid metabolism simulations were conducted with no ontogeny and using the default fast, medium and slow ontogeny profiles within the Simcyp simulator (Figure 8).

Figure 8. Profiles of (A) no ontogeny and (b) fast, (c) medium and (d)slow ontogeny profiles.
Data are shown as a fraction of the enzyme abundance in adults.

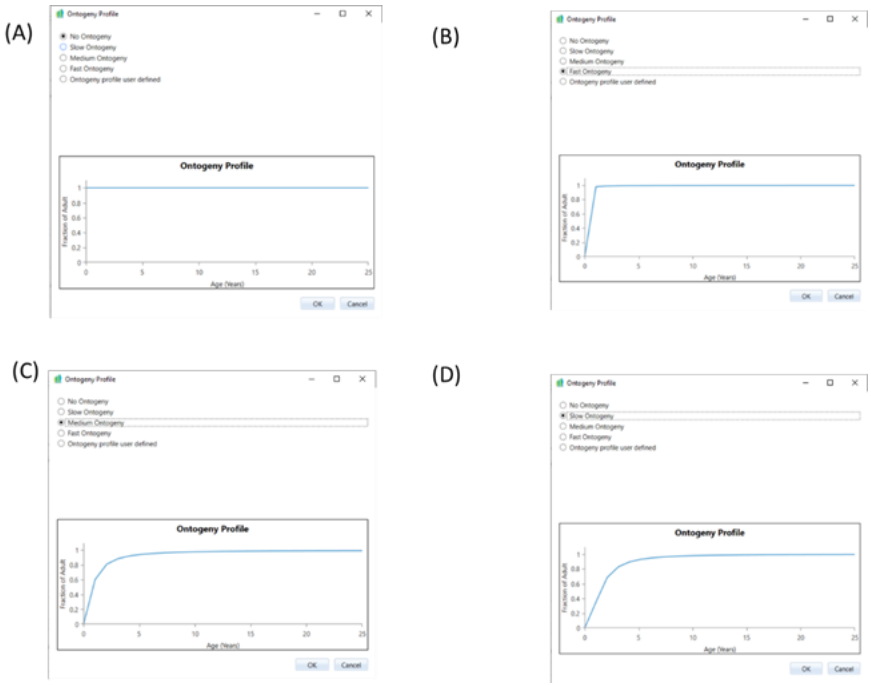

2.1.1.4.3 Intestinal Clearance

Intestinal unbound intrinsic metabolism can be directly scaled from in vitro intestinal microsomal (IM) incubations using a microsomal protein per intestine (MPPI) scaling factor Equation 7.

$$CL_{int,u,G} = CL_{int,u,IM} \cdot MPPI \qquad \text{Equation 7}$$

Where $CL_{int,u,IM}$ is in units of L/h/mg intestinal microsomal protein and $CL_{int,u,G}$ is in units of L/h. CLint,u,G can also be expressed as $Vmax_G/Km_u$. Where Vmax is the maximum rate of metabolism and Km_u is the unbound Michaelis constant.

Alternatively, when the enzyme(s) responsible for metabolic elimination are known along with their absolute abundance, intestinal metabolism can be transformed to a rate per unit enzyme either by normalising observed intrinsic clearance in liver microsomes (LM) (Equation 8) and subsequently scaled on the basis of intestinal absolute enzyme abundance in the intestine (AbundanceGe), or directly scaled from recombinant enzyme data (Equation 9). Metabolism via multiple enzymes can be accounted for by the summation of the respective enzyme contributions (Equation 10).

$$CL_{int,u,enz} = \frac{CL_{int,u,LM}}{Abundance_{Le}} \qquad \text{Equation 8}$$

$$CL_{int,u,G,e} = CL_{int,u,enz} \cdot Abundance_{Ge} \cdot MPPI \qquad \text{Equation 9}$$

$$CL_{int,u,G} = \sum_{e=1}^{n} CL_{int,u,G,e} \qquad \text{Equation 10}$$

Where $CL_{int,u,enz}$ is in units of L/h/pmol enzyme and $CL_{int,u,G}$ is in units of L/h.

When the first order absorption models are used the metabolism in the intestine is estimated using the Qgut model. The Qgut model (Equation 11) can be used to predict intestinal metabolism under the assumption of a homogenous intestinal compartment. Whilst this dramatically simplifies the regional differences in metabolism and transport expression and activities, the Qgut model has been shown a useful approach to predict intestinal metabolism of compounds (40: Yang et al, 2007). The model considers the impact of Qgut, a hybrid parameter consisting of both Qvilli (villus blood flow) and cellular permeability through the enterocyte (CLperm) (Equation 12) and the net intrinsic metabolic clearance in the gut based on unbound drug concentration (CLuint,G) to drive prediction of FG (40: Yang et al, 2007). Utilisation of this strategy provided reasonable predictions for low to medium intestinal extraction drugs using the assumption of fuG (the fraction of drug unbound in the enterocyte) is 1 (i.e. all unbound)(40: Yang et al, 2007, 41: Gertz et al, 2010). However, the predictions were less accurate for drugs with moderate to high intestinal extractions (FG <0.5) (41: Gertz et al, 2010).

$$F_G = \frac{Q_{GUT}}{Q_{GUT} + fu_G \times CLu_{int,G}} \quad \text{Equation 11}$$

$$Q_{GUT} = \frac{Q_{villi} \times CL_{perm}}{Q_{villi} + CL_{perm}} \quad \text{Equation 12}$$

The Advanced Dissolution, Absorption and Metabolism (ADAM) module of the Simcyp Population-Based Simulator® represents the GI tract as seven compartments based upon their physiological and anatomical attributes. The blood flows to each anatomical region of the GI tract are defined separately and the metabolism takes place in various regions of the intestine separately, assuming that each segment is a well-stirred compartment. The regional intestinal metabolism contributions for each compartment of the ADAM model can be calculated by accounting for the distribution of enzymes along the GI tract (Equation 13). Total intestinal metabolism is calculated from the sum of these segmental (Equation 14) and total enzyme contributions (Equation 10).

$$\boldsymbol{CL_{int,u,G,e,i} = CL_{int,u,enz} \cdot Abundance_{Ge,i} \cdot distribution_{G,MPPI} \cdot MPPI} \quad \text{Equation 13}$$

$$\boldsymbol{CL_{int,u,G,e} = \sum_{i=1}^{7} CL_{int,u,G,e,i}} \quad \text{Equation 14}$$

Where $CL_{int,u,G,e,i}$ = intrinsic clearance per pmol enzyme

Abundance $_{Ge,i}$ = abundance per segment (i) in pmol/mg micoromal protein

Distribution$_{G,MPPI}$ = % of microsomal protein per intestine (MPPI)

In the PBPK models developed in this report the intestinal metabolism was considered to be negligible for imidacloprid but CYP3A4 metabolism of acetamiprid in the intestine was accounted for in the model.

Clearance inputs in the rat models

Equivalent *in vitro* metabolic data in rat hepatocytes could not be generated as part of the EU-TOX-RISK project therefore to predict the exposure in the rat the following approach was taken. The *in vivo* clearance predicted in the human simulator was scaled to predict a clearance in rat using a single species scaling approach with an exponent of 0.75 as described by Hosea *et al*. (42: Hosea et al, 2009) (equation 15).

$$CL_{human} = CL_{rat} * \left(\frac{W_{human}}{W_{rat}}\right)^{0.75} \quad \text{Equation 15}$$

Where CL = unbound clearance after intravenous dosing, W = body weight

Excretion

It is possible to account for the excretion of unchanged drug in the kidney or via the biliary system in the PBPK models. In addition to metabolic clearance inputs the PBPK models for imidacloprid, acetamiprid and desnitroimidacloprid contained parameters describing the renal excretion of unchanged drug. Biliary elimination of unchanged drug was not considered within the PBPK models.

General description of equations for eliminating and non-eliminating organs

Each compartment within the full body PBPK model was initially described as a perfusion limited model with representative equations for an eliminating and non-eliminating organ as shown below. The equations describing the behaviour of the compound within the intestine following oral absorption are as described by Jamei at al (20: Jamei et al, 2009). The basic principles for a PBPK model outlined on P19 of the WHO guidance on PBPK modelling were adhered to. Namely

1) the mixing of the chemical in the effluent blood from the tissues is instantaneous and complete;
2) blood flow is unidirectional, constant and non-pulsatile; and
3) the presence of chemicals in the blood does not alter the blood flow rate

In non-eliminating tissues the compound concentration (C) at a given time (t) is defined as follows

$$\frac{dC_{tissue}}{dt} = \frac{Q_{tissue}}{V_{tissue}}\left(C_{ab} - \frac{C_{tissue}}{P_{tissue:p}/_{BP}}\right)$$

Where Q = blood flow to the tissue, V = tissue volume, C_{ab} = arterial blood concentration, BP = blood to plasma ratio and $P_{Tissue:p}$ – partition coefficient of drug between tissues and plasma

In the liver the following equation is applied

$$\frac{dC_{liver}}{dt} = \frac{1}{V_{liver}}\left((Q_{liver} - Q_{pv})C_{ab} + Q_{pv}C_{pv} - \frac{Q_{liver}C_{liver}}{P_{liver:p}/_{BP}} - \frac{f_u}{BP} * \frac{Clu_{int}}{P_{liver:p}/_{BP}} * C_{liver}\right)$$

Where Q_{liver} = sum of blood flow to the liver by the hepatic artery and hepatic portal vein, Q_{pv} = hepatic portal blood vein flow, C_{pv} = hepatic portal compound vein concentration, fu = fraction unbound in plasma, Clu_{int} = intrinsic clearance

Within each simulated animal or human subject the sum of the tissue blood flow rates (excluding the lung) are equal to cardiac output. In line with accepted mammalian physiology the lung also receives a blood flow equal to total cardiac output. Tissue volumes and blood flow rates are within the documented range for each species and age group (paediatric versus adult) considered (14: Jamei et al, 2009, 43: Johnson et al, 2018, 44: Musther et al, 2017).

Population data

Predictions of plasma drug exposure, clearance and other parameters such as fraction metabolised by a particular pathway were made for virtual populations of healthy volunteers. Each population is generated using values and formulae describing demographic, anatomical and physiological variables. Thus, in order to assess clearance predictions in a specific population, data are required for the population variables as well as for the *in vitro* metabolism/transport of the test drug and its observed clearance in the population of interest. The parameter values within the Simcyp Simulator for creating a virtual healthy volunteer population (population, physiological parameters including liver volume and blood flows, enzyme abundances) have been described previously (14: Jamei et al, 2009). The mean value and range of values in a population of 100 healthy adult individuals is given in section 2.1.4.1 (Table 1).

Physiology data used in the healthy human population PBPK populations

Table 1. Mean and range of physiological values generated in a population of 100 Healthy adults (50% female) using an age range of 20-50 as input.
Generated in Simcyp Simulator V19.

Parameter	Mean value	Range
Age (y)	28.7	21 - 50
Weight (kg)	74.8	41 - 119
Height (cm)	169.0	149 - 189
Cardiac output (L/h)	329.5	221 - 420
Serum albumin (g/L)	46.9	38 - 60

For Imidacloprid simulations were also conducted in a population of young children aged 0.24 – 0.26 years old.

Table 2. Mean and range of physiological values generated in a population of 100 Healthy Children (50% female) using an age range of 0.24-0.26 years as input.
Generated in Simcyp Simulator V19.

Parameter	Mean value	Range
Age (y)	0.25	0.24 – 0.26
Weight (kg)	5.5	4.0 - 8.3
Height (cm)	59	54 - 68
Cardiac output (L/h)	36.6	29.7 – 46.7
Serum albumin (g/L)	38.9	29 - 48

Data for simulation of the in vivo kinetics of Acetamiprid, Imidacloprid and Desnitroimidacloprid.

Data and the corresponding source and/or reference used in the PBPK models are shown below.

Acetamiprid

To help with the parameterisation of the PBTK models metabolism of Acetamiprid in human hepatocytes and binding to human plasma and blood was measured *in vitro*. Unfortunately, the metabolism of Acetamiprid was below the limit of quantitation in the standard human hepatocyte suspension stability assay (LOQ ~ 3.86 ml/min/10^6 hepatocytes; Cyprotex unpublished observations) to reliably determine the hepatic intrinsic clearance *in vitro*. In the absence of a measured value for protein binding in the rat a value was calculated assuming the same equilibrium dissociation constant (K_d) for human and rat albumin taking into account differences in the level of serum albumin in rat and human plasma.

PBK models were constructed using full body models in both rat and human where each organ of the body is modelled as a separate compartment. Distribution to tissues was modelled assuming perfusion limited distribution with the tissue:plasma partition coefficients being predicted based on physicochemical data using the method described by Rodgers and Rowland (18: Rodgers and Rowland, 2006). The Kp scalar was adjusted in the rat to bring the predicted concentrations of acetamiprid in line with the observed concentrations for total radioactivity at early timepoints. The same Kp scalar was applied to simulations in human assuming a consistent underprediction of Kp values. The clearance of acetamiprid has not been determined in the rat after oral or intravenous dosing and so a clearance value was used in the simulations that leads to exposure of acetamiprid in the rat that is lower than the total radioactivity exposure at a dose of 1 mg/kg ^{14}C-acetamiprid. A sensitivity analysis is shown to illustrate the effect of changing the clearance of acetamiprid over a 100-fold range.

Oral absorption of acetamiprid in rat and human models was predicted using a permeability value predicted from an *in vitro* determined Papp value in Caco-2 cells together with the solubility of acetamiprid. Oral absorption was predicted using the advanced, dissolution, absorption and metabolism (ADAM) model within the Simcyp simulator (20: Jamei et al, 2009).

The human clearance of Acetamiprid has not been defined. The clearance used in the human model was calculated using a clearance value in rat (0.7 ml/min) that gave exposure in line with the total radioactivity observed in rat plasma following oral dosing of ^{14}C-acetamiprid. The human clearance was allometrically scaled using a single species approach and an exponent of 0.75 (equation 1). This clearance was then partitioned into metabolic and renal CL with the renal CL defined as ~2.6% of the total CL based on the data in Harada *et al*. (4: Harada et al, 2016). The metabolic CL was arbitrarily split into metabolism by CYP

3A4 (~80%) resulting in formation of desmethyl acetamiprid and metabolism not forming the metabolite (~20%).

The N-desmethyl metabolite was also simulated in the human PBTK model. As for parent compound Vss and Kp values were predicted using the method described by Rodgers and Rowland (18: Rodgers and Rowland, 2006). Clearance was calculated based on the half-life of renal excretion of desmethylacetamiprid observed in the study conducted by Harada (4: Harada et al, 2016) and the predicted volume of distribution. The split between renal and hepatic CL for the metabolite was calculated based on the calculated amount of acetamiprid ingested in the diet and the observed urinary excretion of desmethylacetamiprid in the study reported by Harada (4: Harada et al, 2016).

Input parameters for the PBK models Acetamiprid (rat and human)

Parameter	Value	Reference
Molecular Weight	222.7	Pubchem
Log P	0.8	(1: Brunet et al, 2008)
Compound Type	Neutral	
Blood:plasma ratio	0.951	Measured
Fraction unbound in plasma	0.719	Measured
Intestinal permeability		
Caco-2 cell A-B (papp)	26 x 10^{-6} cm/s	(1: Brunet et al, 2008)
Solubility	4.25 mg/mL	Pubchem
Distribution		
Vss	Predicted Rat 0.80 L/kg Human 0.69 L/kg Kp scalar 1.3	(18: Rodgers and Rowland, 2006) Kp scalar use dto ensure that predicted concentrations in the rat were in line with measured concentrations of total radioactivity.
Brain Kp	0.5 rat (predicted 1.07) 1.2 Predicted (human)	Modifed in rat to be in line with the measured data in mouse (2: Ford and Casida, 2006)
Clearance	Rat 1.3 ml/min 0.08 ml/min renal CL Human 0.082 L/h renal CL	 5-7% excreted as unchanged drug Assumed that metabolism is by CYP 3A4 -allows metabolite formation to occur. Arbitrarily ~80% of the acetamiprid is metabolised to the desmethyl metabolite. Based on 2.6% excretion in human urine 2.6% excreted in urine (4 : Harada et al, 2016)

N-desmethyl metabolite (human only)

Parameter	Value	Reference
Molecular Weight	209	Pubchem
Log P	1.3	Pubchem
Compound Type	Neutral	Assumed
Blood:plasma ratio	1	Assumed
Fraction unbound in plasma	0.719	Assumed same as parent
Distribution		
Vss	Predicted Human 1.11 L/kg Kp scalar 1.3	(18: Rodgers and Rowland, 2006) Assumed the same as human
Clearance	Hepatic 0.201 μl/min/mg	Split between hepatic and renal CL calculated using data from (4 : Harada et al, 2016)

	Renal 0.95 L/h	

Imidacloprid

To help with the parameterisation of the PBK models metabolism of imidacloprid in human hepatocytes and binding to human plasma and blood was measured *in vitro*. Unfortunately, the metabolism of imidacloprid was below the limit of quantitation in the standard human hepatocyte suspension stability assay (LOQ ~ 3.86 ml/min/10^6 hepatocytes; Cyprotex unpublished observations) and in a low clearance assay format (LOQ ~0.143 ml/min/10^6 hepatocytes) to reliably determine the hepatic intrinsic clearance *in vitro*. In the absence of a measured value for protein binding in the rat a value was calculated assuming the same equilibrium dissociation constant (K_d) for human and rat albumin taking into account differences in the level of serum albumin in rat and human plasma.

PBK models were constructed using full body models in both rat and human where each organ of the body is modelled as a separate compartment. Distribution to tissues was modelled assuming perfusion limited distribution with the tissue:plasma partition coefficients being predicted based on physicochemical data using the method described by Rodgers and Rowland (18: Rodgers and Rowland, 2006). Initially the clearance of imidacloprid in the rat PBK model was determined based on the reported data from Kapoor et al., (5: Kapoor et al, 2014). A sensitivity analysis approach was used to find a range of clearance values in the rat whereby the simulated exposure of imidacloprid was less than the total radioactivity observed in plasma following oral dosing of 14C- labelled imidacloprid to male rats.

Oral absorption of acetamiprid in rat and human models was predicted using a permeability value predicted from an in silico mechanistic permeability model (Sugano 2009 (29)) together with the solubility of imidacloprid. Oral absorption was predicted using the advanced, dissolution, absorption and metabolism (ADAM) model within the Simcyp simulator (20: Jamei et al, 2009).

The human clearance of imidacloprid has not been defined. The clearance used in the model was calculated based on the predicted Vss and the reported half-life for excretion of deuterated imidacloprid in urine after oral dosing of 5 mg to human subjects (4: Harada et al, 2016). The renal CL of imidacloprid was assigned based on the finding that 12-13% of the dose of deuterated imidacloprid was recovered unchanged in human urine over 96 hours following oral administration of 5 mg of deuterated imidacloprid (4: Harada et al, 2016). As different values of Vss and clearance can give the same half-life the effect of using different pairs of values was also investigated.

Input parameters for the PBK models

Imidacloprid (rat and human)

Parameter	Value	Reference
Molecular Weight	255.7	Pubchem
Log P	0.57	
Compound Type	Neutral	
Blood:plasma ratio	1 (rat) 0.954 (human)	Measured Assumed Measured
Fraction unbound in plasma	0.79 (rat) 0.724 (human)	Measured Calculated Measured
Intestinal permeability		
MechPeff model (Ptrans,0 10^{-6} cm/s)	41.7	(29:Sugano 2009)

Solubility	0.61 mg/ml	Pubchem
Supersaturation Ratio	100	To ensure fa is consistent with observed data for radioactivity.
Distribution		
Vss	0.59 L/kg (rat) 0.49 L/kg (human)	(18: Rodgers and Rowland, 2006)
Brain Kp	0.74 (rat) 0.78 (human)	Predicted
Clearance	Rat 5OH Vmax 159 pmol/min/mg Km 38.4 μM Additional Cl 6 ml/min Renal CL 0.58 ml/min Human HLM 0.228 μl/min/mg Renal CL 0.097 L/h	(7: Kolanczyk et al, 2020) Based on excretion of unchanged imidacloprid in rat Adjusted to give a half-life of ~35 hours (in line with the urinary excretion data). Renal CL assigned based on recovery of deuterated imidacloprid in urine as reported by Harada et al.(4: Harada et al, 2016).

Desnitroimidacloprid

A PBPK model for desnitroimidacloprid was established in the Simcyp simulator V20. Due to the lack of published human metabolism and exposure data for desnitroimidacloprid an analogue approach was used to inform the PBPK model using a compound (atenolol) with known human pharmacokinetics and similar physicochemical properties. In studies conducted with desnitroimidacloprid in a hepatocyte co-culture system the measured *in vitro* intrinsic clearance was <0.143 ml/min/10^6 cells (i.e. below the limit of quantitation of the assay; in the same experiment the positive control compounds ketoprofen and prednisolone had measured intrinsic clearance values of 4.39 and 0.379 , ml/min/10^6 cells respectively).

As an analogue of desnitroimidacloprid atenolol a compound with similar physicochemical properties was used. The input parameters for Desnitroimidacloprid and Atenolol are given in the table below.

Input parameters for the Desnitroimidacloprid and atenolol PBK models

Parameter	Desnitro -imidacloprid (DNI)	Atenolol	Source
Molecular weight (g/mol)	210.7	266.3	Pubchem
log P	0.23	0.25	DNI average of 6 estimates from different sources.
Compound type	Monoprotic base	Monoprotic Base	
pKa	9.6	9.6	DNI average of values in CHEMBL and ACD. Atenolol value taken from Dahlgren et al., 2016.(45)
B/P	0.759	1.07	DNI measured. Atenolol taken from Taylor et al., 1981.(46)
fu	0.841	0.97	DNI measured. Atenolol data taken from Barber et al., 1978.(47)

Main plasma binding protein	Human serum albumin	Human Serum albumin	assumed
Absorption parameters Jejunal permeability (10^{-4} cm/s)	0.63	0.45	Predicted – mechanistic permeability model (Sugano 2009 (29)). For atenolol the p,trans 0 value was calibrated so that the jejunal permeability corresponded to the observed value in humans reported by Dahlgren et al. The same calibration to p,trans 0 was applied to DNI
$P_{trans,0}$ (10^{-6}cm/s)	120	120	
fu_{gut}	1	1	
Distribution Model	Full PBPK Model		
V_{SS} (L/kg)	0.85	0.88	Predicted - Method 2 (Rodgers and Rowland, 2006). Atenolol value adjusted to be in line with the value reported by Dahlgren et al., 2016 (45)
Metabolic Clint CYP3A4 (ml/min/pmol enzyme)	0	0.00073	Atenolol is 95% excreted into urine
CL_R (L/h)	3.2	9.64	Predicted using Mech Kim model (Burt et al., 2016)(48). Atenolol CL_R was adjusted to recover the mean CL_R reported after IV dosing by Kirch (49), Mason (50), Wan (51).

Results

Acetamiprid

Due to the paucity of the data available to construct the PBTK models for acetamiprid and its desmethyl metabolite there is significant uncertainty in many of the parameters used within the PBPK model. In the rat available concentration data included data on total radioactive concentrations following dosing of a 1 mg/kg dose to rats. The maximal concentrations of acetamiprid that can be achieved in the rat are the measured radioactivity concentrations but as acetamiprid is extensively metabolised it is likely that the concentrations of acetamiprid are lower than those of total radioactivity particularly at later timepoints. The simulated concentrations of acetamiprid after an oral dose of 1 mg/kg to rats is shown in Figure 28. The predicted absorption (fa=1) of acetamiprid in the rat is in line with experimental data.

Sensitivity analysis showed that decreasing the clearance of acetamiprid by a factor of 2 or increasing it by a factor of 10 both gave results that are consistent with observed data (Figure 2). Further decreasing the clearance of acetamiprid within the model resulted in concentrations that were higher than the observed total radioactivity seen in rat plasma following an oral dose. This is illustrated in Figure 29 with a simulation where the clearance was decreased 10-fold. Using this approach, a lower limit for clearance of acetamiprid in rat can be estimated but it is not possible to say which value higher than this is the correct one.

Figure 9. Simulated (green line) concentrations of acetamiprid in plasma following an oral dose of 1 mg/kg to male rats.

Observed data (orange and grey dots) are for total radioactivity after administration of 1 mg/kg doses of 14C-acetamiprid labelled on the ring (orange) or CN group (grey). Data is taken from the RAR_08 document Table B.6.1.1.1-1. Panel B shows the data with the y-axis on a Logarithmic scale.

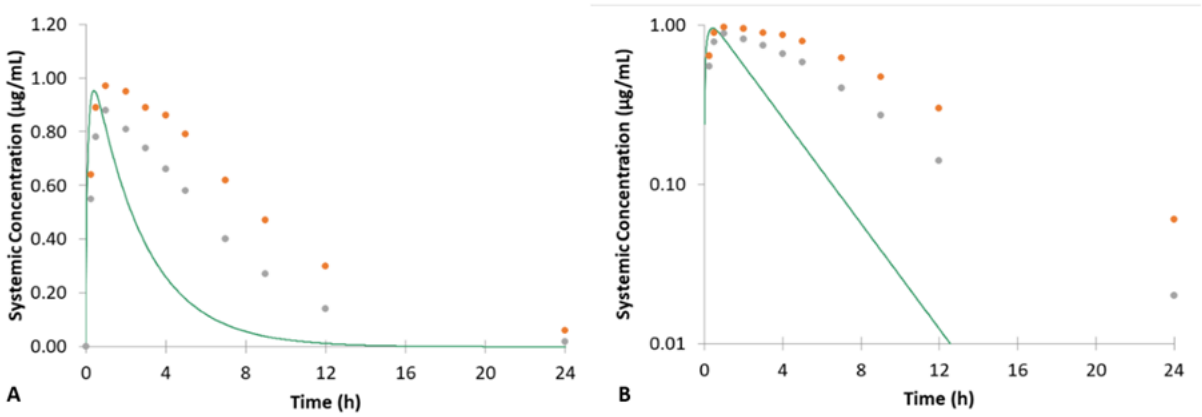

Figure 10. Sensitivity analysis showing the effect of changing clearance on plasma concentrations of Acetamiprid following an oral dose of 1 mg/kg to male rats.

Clearance was the same as in figure 1 and Table 1 (green line) or decreased by a factor of 2 (blue) or 10 (black) or increased by a factor of 10 (red). Observed data (orange and grey dots) are for total radioactivity after administration of 1 mg/kg doses of 14C-acetamiprid labelled on the ring (orange) or CN group (grey). Data is taken from the RAR_08 document Table B.6.1.1.1-1. Panel B shows the data with the y-axis on a Logarithmic scale.

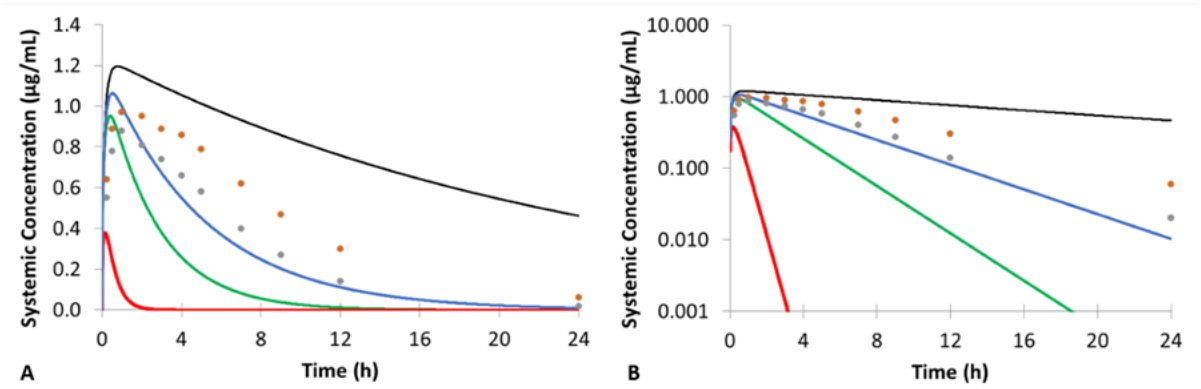

The simulated levels of acetamiprid and the desmethyl metabolite following an oral dose of 5 µg acetamiprid in human plasma (Figure 30) and the cumulative urine excretion (Figure 31 and 32) are shown below. Although part of the metabolism of acetamiprid in the human PBK model was assigned to CYP3A4 an enzyme known to be expressed in the intestine the low rates of metabolism assigned to the enzyme result in 98% of the absorbed drug escaping from first pass metabolism in the gut (Fg = 0.98) and as such the compound is predicted to have high bioavailability >90% after oral dosing in humans.

Figure 11. Simulated mean plasma concentration of acetamiprid (green) and the desmethylmetabolite (orange) in humans after an oral dose of 5 µg acetamiprid.

Simulations were conducted in 100 North European Caucasian subjects (aged 20-50; 50% female).

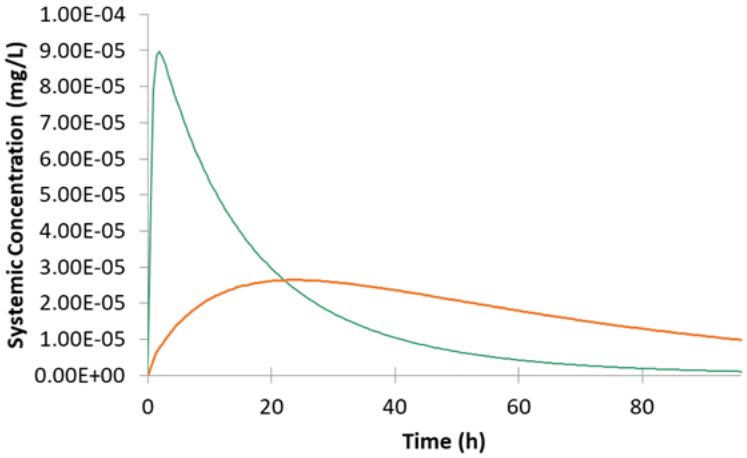

Figure 12. Simulated cumulative urinary excretion of (A) acetamiprid and (B) the desmethylmetabolite in humans after an oral dose of 5 μg acetamiprid.

Simulations were conducted in 100 North European Caucasian subjects (aged 20-50; 50% female). The green line represents the mean simulated cumulative renal excretion and the dashed black lines the 5th and 95th percentile of the population. The orange squares in panel B represent the observed data from Harada et al.

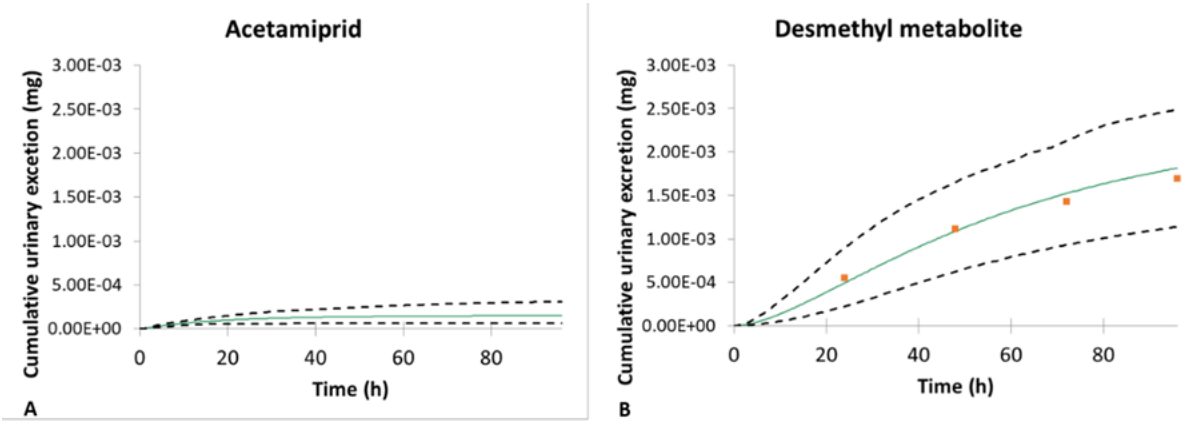

Figure 13. Simulated mean cumulative urinary excretion of the desmethyl metabolite in humans after an oral dose of 5 μg acetamiprid.

Simulations were conducted in 100 North European Caucasian subjects (aged 20-50; 50% female) (green line) and in 100 Japanese subjects (aged 20-50; 50% female) (grey line). The orange squares represent the observed data from Harada et al.(4)

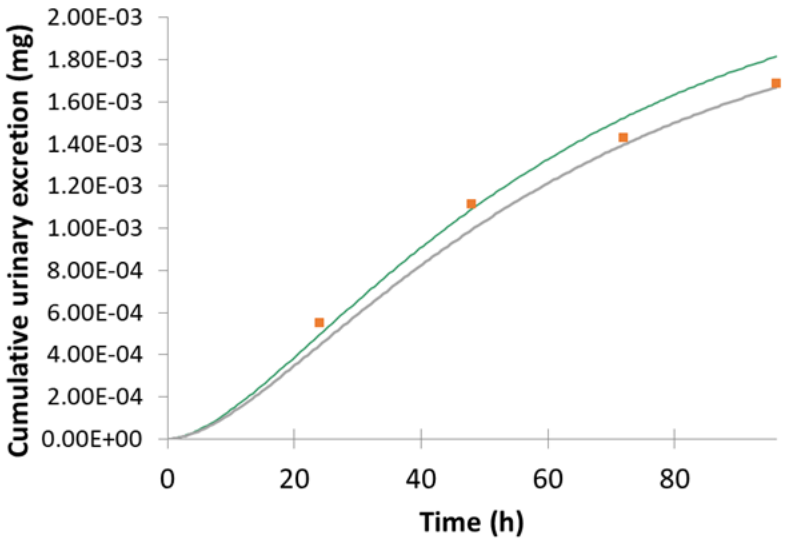

As there is not much data to verify the PBTK model the effect of changing the clearance of acetamiprid on the simulated renal excretion of the desmethyl metabolite was investigated. Simulations were conducted in a population of 100 Japanese subjects (aged 20-50; 50% female) (Figure 33). Changing clearance of acetamiprid over a 100-fold range results in changes in the simulated plasma concentrations of acetamiprid

(Figure 33A) with higher concentrations at lower clearances. Increasing the clearance leads to an earlier maximum plasma concentration for the metabolite while decreasing clearance leads to a later time for maximum concentration and lower maximal concentrations of the metabolite. Compared to the observed renal excretion of the metabolite making the clearance of acetamiprid higher has a minimal impact on the time course of metabolite renal excretion as the elimination is mainly controlled by the intrinsic properties within the metabolite PBK model (Figure 33C). Lower clearances of acetamiprid lead to an underprediction of the renal excretion of desmethyl metabolite and suggest that while it is possible that the clearance of acetamiprid is faster than the values used in the base model (Table 2) it is less likely to be significantly slower as this would lead to the renal excretion of the metabolite being inconsistent with the observed data.

Figure 14. Simulated mean plasma concentrations of (A) acetamiprid and (B) desmethylacetamiprid and (C) cumulative renal excretion of desmethylacetamiprid in humans after an oral dose of 5 μg acetamiprid.

Simulations were conducted in 100 Japanese subjects (aged 20-50; 50% female). The green line represents the simulation with the baseline clearance value for acetamiprid and the blue line is a 10-fold decrease in clearance and the black line a 10-fold increase in clearance. No alterations were made to the PBTK model of desmethylacetamiprid. The orange squares represent the observed data from Harada et al.(4)

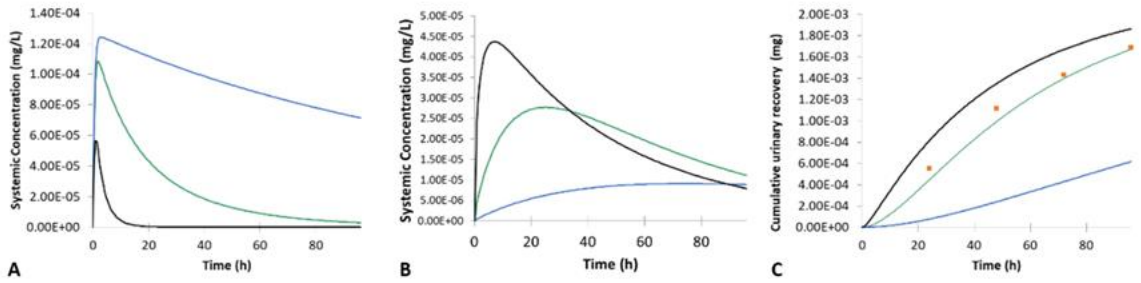

Simulations using the Acetamiprid PBTK model

As the metabolite of acetamiprid is not of toxicological concern simulations in different scenarios only show the data for parent acetamiprid. To make it easier to put the concentrations in context with the *in vitro* data concentrations are reported in μM or nM concentration units.

The simulated exposure in rats doses with 1 or 50 mg/kg/day Acetamiprid is shown in Figure 34. The maximal concentrations are in the low to mid μM range dependent on dose. Besides the effect of solubility there are no non-linear mechanisms eg saturation of clearance accounted for within the PBTK models. The predicted C_{max} is in line with the maximal concentration of total radioactivity seen in blood after dosing male rats with 50 mg/kg of labelled acetamiprid (~180 μM).

The simulated exposure in humans (0.114/mg/kg/day) is shown in Figure 35. To reach a Cmax in plasma of 1μM (where activation of the receptor nAChRs have been observed in the SH-SY5Y cells, it would require an oral dose of 0.1-0.2 mg/kg which is 4-10 times higher than the acute reference dose (0.025 mg/kg/day)[12]. Using the PBTK model to run a simulation in a population of 100 individuals (aged 20-50; 50% female) a dose of 15 mg/kg/day gives a mean unbound maximum acetamiprid concentration in plasma of 84 μM (58-129 μM 5th and 95th percentiles). Activation of nAChRs does not affect human neurodevelopment (KE4) up to at least 100 μM. The dose of 15 mg/kg/day is 600 times higher than the acute reference dose (0.025 mg/kg/day).

Figure 15. Simulated plasma (green) and brain (black) concentrations of Acetamiprid in rats after multiple oral doses of (A) 1 mg/kg/day and (B) 50 mg/kg/day.

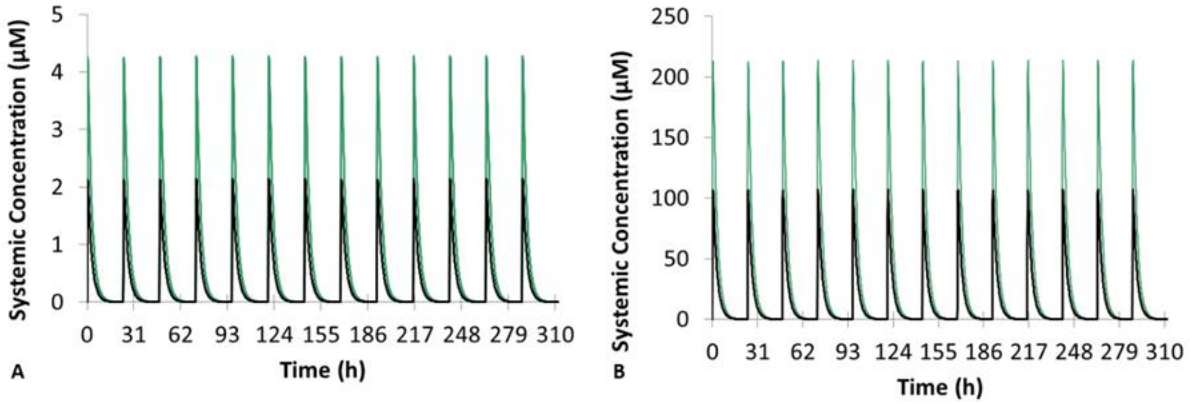

Figure 16. Simulated (A) plasma and (B) brain concentrations in human subjects after multiple oral doses of 0.114 mg/kg/day for 10 days.

The mean concentration is represented by a green line and the 5th and 95th percentiles by dashed black lines. Simulations were conducted in a population of 100 North European Caucasian healthy subjects (age 20-50; 50% female).

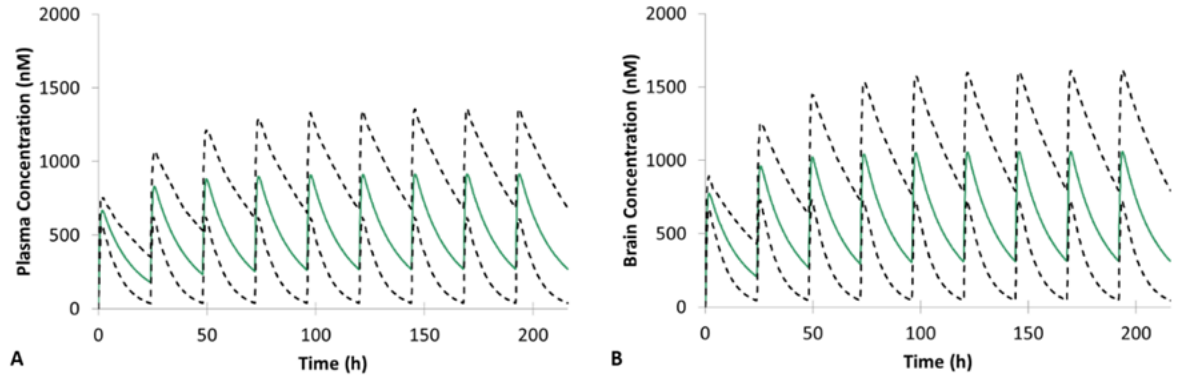

Imidacloprid

The PBK model for imidacloprid was constructed initially in the rat. The distribution of imidacloprid to rat tissues was predicted using the algorithms proposed by Rodgers and Rowland (18). The predicted brain:plasma ratio using this method is in line with experimental data in the mouse and within 2-fold of the brain:blood ratio reported by Kapoor *et al*.(5) Initial simulations using either *in vitro* metabolism data reported by Kolanczyk *et al* (not shown)(7) or the calculated oral clearance of imidacloprid (0.83 ml/min) over-predicted the exposure of imidacloprid when compared to total radioactivity levels in the plasma of male rats dosed with 20 mg/kg ^{14}C-Imidacloprid (Figure 25). To bring the exposure of imidacloprid in line with the total radioactivity levels clearance of the compound was increased (Figure 25; Table 3). The clearance of Imidacloprid may be faster than the values used here as there is significant uncertainty in the true value of Imidacloprid clearance in the rat. The exposure and clearance of imidacloprid reported in female rats by Kapoor *et al*.(5) are inconsistent with the levels of total radioactivity reported in the DAR. Whether this represents a sex difference or is an effect of the corn oil vehicle used by Kapoor *et al*.(5),

resulting in flip-flop pharmacokinetics and higher exposure is not clear. Although the delayed Tmax seen in the study by Kapoor *et al*.(5) is consistent with the second hypothesis.

Figure 17. Simulated (green line) concentrations of imidacloprid in plasma following an oral dose of 20 mg/kg to male rats.

Observed data (orange dots) are for total radioactivity after administration of 20 mg/kg doses of 14C-imidacloprid. Data is taken from the RAR document Table B.6.1-22. Panel B shows the data with the increased clearance values shown in Table 3.

(A) (B)

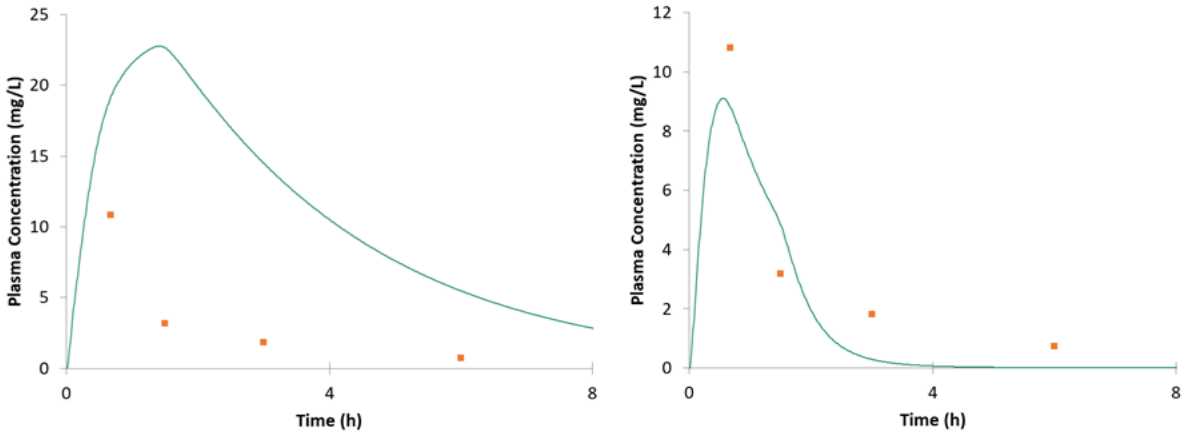

There is significant uncertainty in the input values for the rat PBK model and other values of Vss and combinations of Vss and clearance could equally give results consistent with the observed data which are based on total radioactivity after dosing of ^{14}C-imidacloprid. As is shown in figure 26 as an example increasing the Vss by a factor of 2 or decreasing it be a factor of ~3 also produces results consistent with the observed data.

Figure 18. Simulated concentrations of imidacloprid in plasma following an oral dose of 20 mg/kg to male rats.

The green line shows simulations using identical input parameters to the simulation in figure 25B (higher clearance value and kp scalar =1. The blue line shows a PBK model with a lower volume of distribution kp scalar =0.3. The grey line shows simulations with the same value of clearance but a larger volume of distribution. The Kp in each tissue apart from the brain was increased by a factor of 2. The brain distribution was unchanged ~0.75 to remain in line with measured brain:plasma ratio. Observed data (orange dots) are for total radioactivity after administration of 20 mg/kg doses of 14C-imidacloprid. Data is taken from the DAR document Table B.6.1-22. Panel B shows the data with the y axis on a logarithmic scale.

(A) (B)

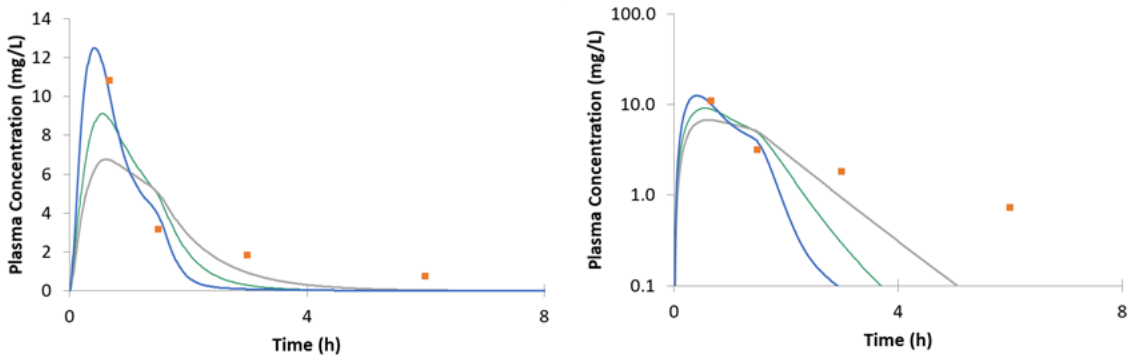

In humans the urinary excretion of deuterated imidacloprid has been measured following an oral dose of deuterated imidacloprid (4). In the absence of other data, the data from Harada *et al*.(40 was used to assess the performance of the PBK model under the assumption that the disposition of imidacloprid and the deuterated analogue are the same. Using the parameters outlined in table 3 it is possible to produce a PBK model that is consistent with the observed data (Figure 27).

Figure 19. Simulated plasma concentration (A) and (B) urinary excretion of imidacloprid in humans after an oral dose of 5 μg imidacloprid.

Simulations were conducted in 100 North European Caucasian subjects (aged 20-50; 50% female). The green line represents the mean simulated data and the dashed black lines the 5th and 95th percentile of the population. The orange squares in panel B represent the observed data from Harada et al.

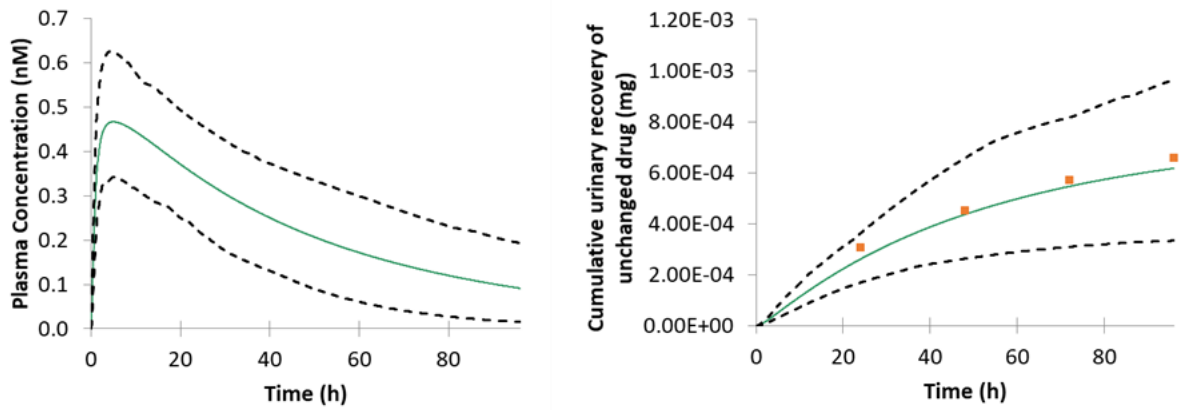

With only urinary excretion data after oral dosing available to verify the performance of the model there are different combinations of clearance and volume input parameters that can produce simulation results in line with the observed renal excretion data. This is illustrated in Figure 4 where the Vss used as input in the model is varied over a range of 0.3 to10 times the original values presented in Table 3. This was achieved by varying the kp scalar over a range of 0.3 to 10. At the higher values of kp scalar the brain:plasma ratio was kept constant at 0.75 to be consistent with the experimental data in mice. For each simulation, the renal excretion was kept constant at 12.7% of total clearance and the overall clearance varied to maintain a half-life of ~35 hours. The simulations were run in a population of individuals but only mean data is shown for clarity. As can be seen in figure 28 varying the input parameters changes the plasma concentration of imidacloprid significantly but has minimal impact on the urinary recovery of the compound.

Figure 20. Simulated mean plasma concentration (A) and (B) urinary excretion of imidaloprid in humans after an oral dose of 5 μg imidacloprid.

Simulations were conducted in 100 North European Caucasian subjects (aged 20-50; 50% female). The different coloured lines represent different PBK models where the Vss and clearance were varied. The green line is the baseline model (Table 3) with a kp scalar of 1, the black line kp scalar = 0.3, blue kp scalar = 2, red, kp scalar =5, purple kp scalar =10. The orange squares in panel B represent the observed data from Harada et al.(4)

(A)

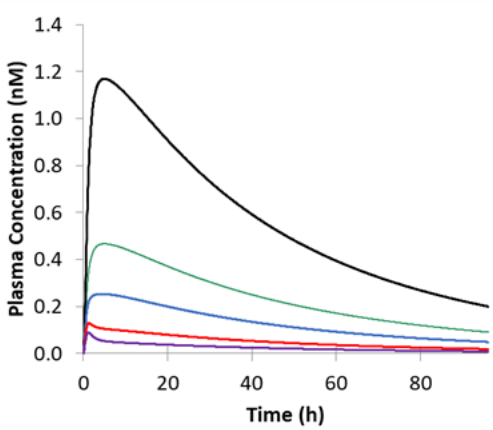

(B)

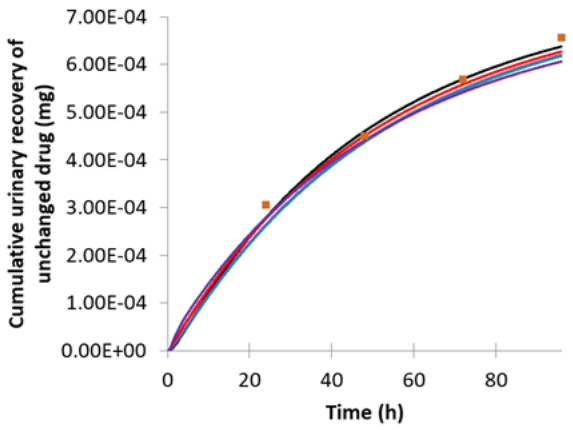

To keep the half-life constant in the simulations shown in figure 28 the clearance is increased in parallel with the increasing volume of distribution. At the higher volumes (increased by 5 or 10-fold) the metabolic clearance needed within the model reaches a point when it should be observable in the *in vitro* assays that were conducted for the project. This suggests that the most likely combinations of parameters are when the predicted Vss of imidacloprid are <0.85 L/kg. This level of distribution within the body is consistent with a permeable compound that widely distributes through the whole-body water without extensively binding to tissues. This is consistent with the physicochemical and *in vitro* properties of imidacloprid. For instance, in the Caco-2 cell line the permeability of imidacloprid has been measured to be 21.6 x 10^{-6} cm/s consistent with a highly permeable compound (1).

The simulated exposure in humans (0.16/mg/kg/day; corresponding to a maximally expected level in the normal population) is shown in Figure 29. This intake scenario would lead to brain concentrations of 0.5-1.2 μM (Figure 29). Applying reverse modelling revealed, that a brain concentration of 2 μM imidacloprid (considered a point-of-departure from our in vitro studies) would be reached after an intake of 0.2 mg/kg

body weight in the average population. Importantly, desnitro imidacloprid was found to be more than 10x more potent than imidacloprid in our studies.

Figure 21. PBTK modeling of imidacloprid concentrations in a human population exposure scenario

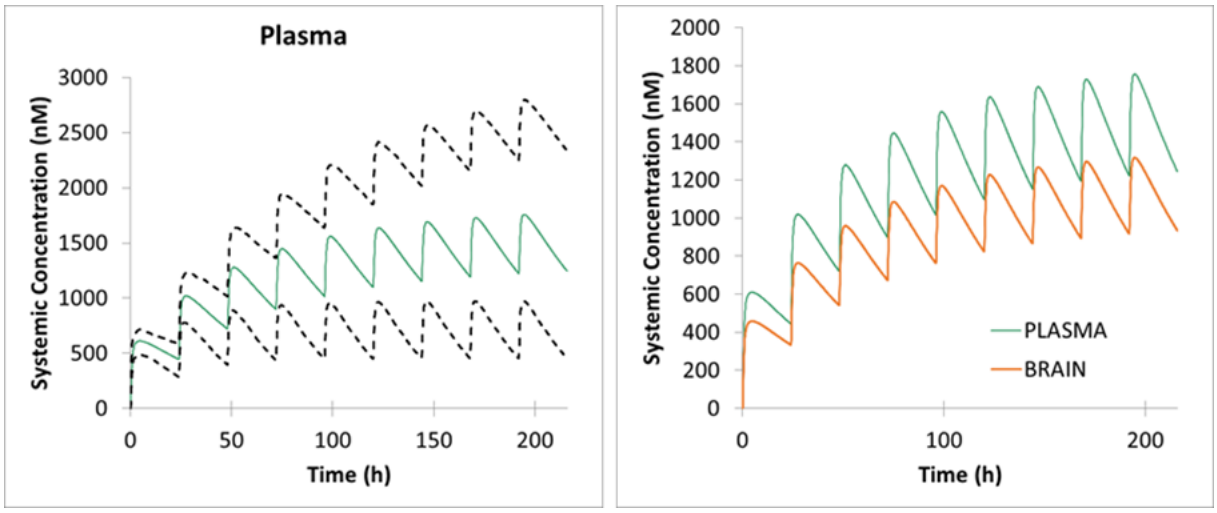

Simulations with a dose of 0.16 mg/kg/day were also undertaken in a population of pregnant female subjects the mean results were similar to those seen in the non-pregnant population of healthy volunteers (HV) (Figure 22)

Figure 22. PBTK modeling of imidacloprid concentrations in pregnant and non-pregnant (HV) adult human population exposure scenarios

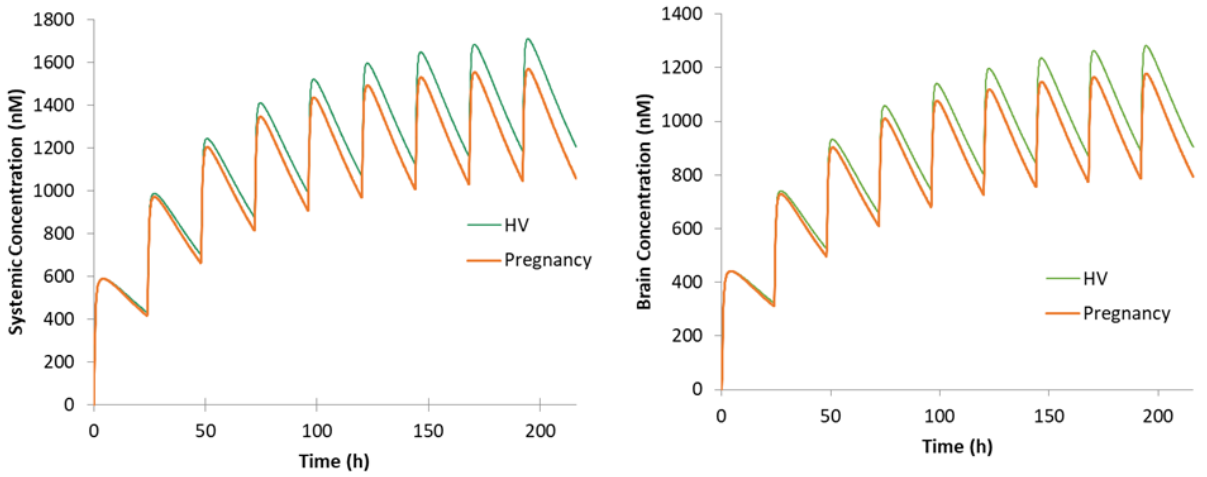

Although there is uncertainty in the enzymes involved in the metabolism of imidacloprid in humans simulations were also conducted in a population of young children (age range 0.24 -0.26 years) exposed to a dose of imidacloprid of 0.16 mg/kg/day. Because the enzymology of imidacloprid metabolism is uncertain the change in metabolism of imidacloprid with age in children is also uncertain. To exemplify this different ontogeny profiles were simulated – assuming no ontogeny i.e. the enzyme level per mg protein is the same in adults and children and the fast, medium and slow ontogeny functions within the Simcyp

simulator. If specific enzymes involved in the metabolism of imidacloprid are identified then the ontogeny of these specific enzymes can be incorporated in the simulations.

Figure 23. PBTK modelling of imidacloprid concentrations in adults (HV) and children (aged 0.24 – 0.26 years) exposed to an imidacloprid dose of 0.16 mg/kg/day.
In the children 4 different ontogeny profiles were simulated.

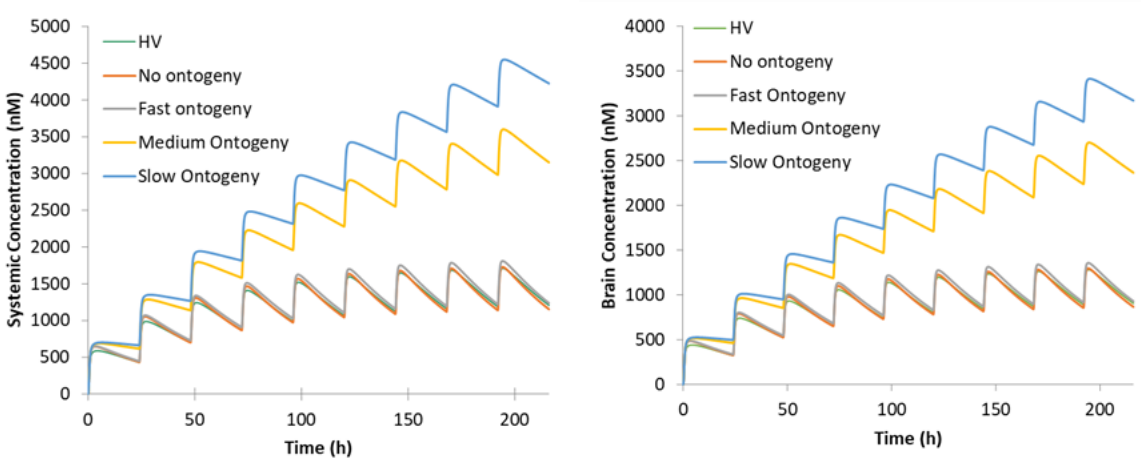

Desnitroimidacloprid

Figure 24. PBTK modelling of desnitroimidacloprid concentrations in adults exposed to a desnitroimidacloprid dose of 0.016 mg/kg/day given every 24 hours.
In the simulation 100 individuals aged 20:50 (50% female) were used. The green line represents the mean data and the dashed lines represent the 5th and 95th percentiles of the population.

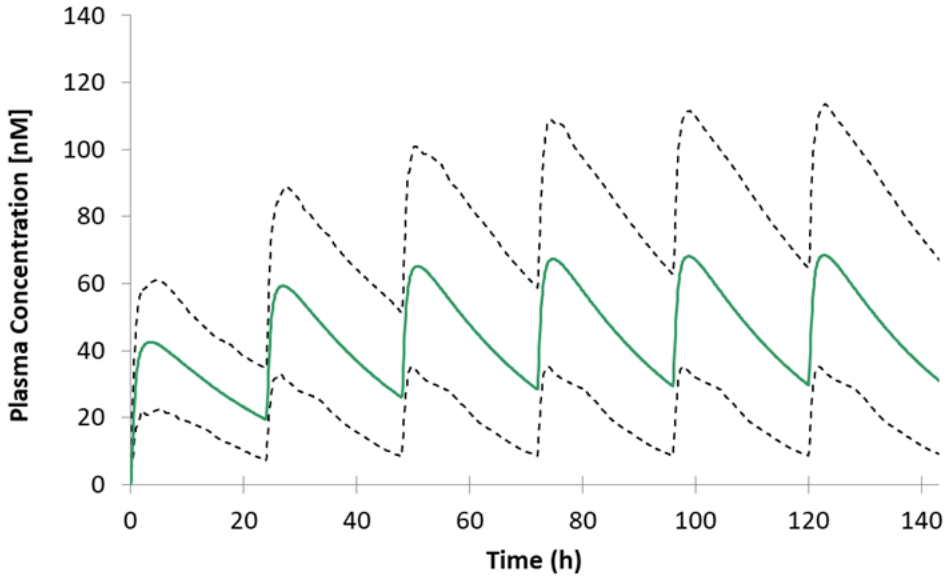

As the rate of metabolism of desnitroimidacloprid was below the limit of quantitation of the clearance assay no metabolic clearance was included in this desnitroimidacloprod PBPK model. This is a conservative assumption and metabolism components can be included in the model if data becomes available. Renal clearance for desnitroimidacloprid was assumed to be governed only by passive processes with both filtration and passive reabsorption being accounted for. Passive permeability was scaled from the predicted permeability in the intestine (Peff 0.37 10^{-4} cm/s) accounting for the surface area of the proximal tubules in the kidney. The renal CL for atenolol also includes a component of active secretion and was entered into the model using the reported transporter kinetic data in Yin *et al* 2015 (PMID: 26374172). In the absence of equivalent data for desnitroimidacloprid no active secretion component was included for this compound. If active secretion does occur for desnitroimidacloprid this would result in a lower exposure of DNI in the body.

Atenolol

Figure 25. PBTK modelling of Atenolol concentrations in adults dosed with multiple doses of 50mg per day.

The green line is the mean concentration and the black dashed lines the 5th and 95th percentiles of the total population. In this study 10 trials of 16 subjects aged 36-65; 31% female were run. Observed data from Andrawis et al (J Clin Pharmacol., 2000, 40, 231) are shown as purple circles. The simulated mean atenolol, Cmax and AUC were 245 ng/mL and 2867 ng*h/mL and are in reasonable agreement with the reported mean values (409.3 ng/mL for Cmax and 3534 ng*h/mL for AUC). The simulated Cmax and AUC were within 1.7 and 1.2 fold of the observed values from this clinical study and were considered to be adequate for the purposes of this exercise

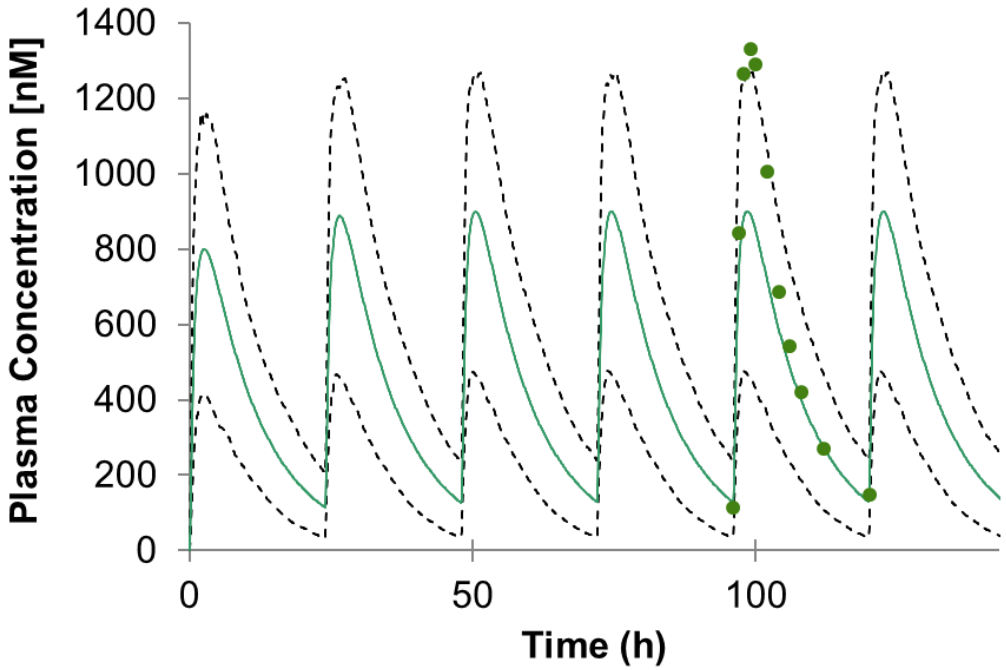

Discussion

Using the available data the plasma concentrations of acetamiprid and imidacloprid were simulated in humans and rats. For model verification in humans urine excretion of deuterated acetamiprid, the desmethyl metabolite of deuterated acetamiprid and imidacloprid was used. This is based on an assumption that deuteration to allow detection by LC-MS/MS does not alter the clearance of the compound. As only urine data was available and there were no measured blood concentrations different clearance and volume parameters could give the same result. This adds significant uncertainty to the modelling of these compounds that it is difficult to fully resolve without more observed data.

The predicted brain concentrations for the compound were calculated using a tissue:plasma partition coefficient (Kp). These values were predicted but in reasonable agreement with observed data in pre-clinical species. The compounds had low protein and tissue binding with total brain concentrations predicted to be a bit lower than total plasma concentrations.

Initially the rate of imidacloprid metabolism to form desnitroimidacloprid was going to be incorporated into the model to allow the concentrations of the metabolites to be simulated. However, in all of the *in vitro* experiments conducted as part of the project it was not possible to show formation of desnitroimidacloprid from imidacloprid. These results contrast with literature reports but the reasons for the different findings in unclear. Due to the lack of metabolism observed it was not possible to parameterise a model whereby imidacloprid was metabolised to desnitroimidacloprid. The only metabolites detected in the *in vitro* incubations were hydroxylated and olefin metabolites. Although desnitroimidacloprid has been detected in some human biomonitoring studies the compound is formed be degradation and plant metabolism and is known to be present in food consumed by humans treated with imidacloprid. It is not clear therefore how much (if any) of the desnitroimidacloprid found in human urine biomonitoring studies arises from metabolism of imidacloprid.

Conclusions

Model Evaluation Aspect	Observation
Biological basis	The structure of the human and rat PBPK models are consistent with known physiology. The tissue volumes and blood flow are consistent with measured values from the literature.
Model simulations of data	There is limited observed data available for comparison. PBPK models were constructed for all of the compounds and were consistent with the small amount of observed data available. The atenolol compound file produced results consistent with observed clinical data.
Reliability (model testing, uncertainty and sensitivity)	Due to issues with identifiability and only having urine excretion data to compare the PBPK model results against different combinations of clearance and volume parameters could produce results consistent with the observed data. Thus there is significant uncertainty about the true volume and clearance of the compounds. In this work more conservative but physiologically reasonable parameters were used to simulate the different exposure scenarios.

References

Berezhkovskiy. (2004), “Volume of distribution at steady state for a linear pharmacokinetic system with peripheral elimination.”, *J Pharm Sci.*, Vol. 93(6), pp. 1628-40. [49]

Brouwers J, B. (2009), “Supersaturating drug delivery systems: the answer to solubility-limited oral bioavailability?”, *J Pharm Sci.*, Vol. 98(8), pp. 2549-72. [28]

Brown HS, C. (2007), “Use of isolated hepatocyte preparations for cytochrome P450 inhibition studies: comparison with microsomes for Ki determination.”, *Drug Metab Dispos.*, Vol. 35(11), pp. 2119-26. [29]

Brunet JL, M. (2008), *Intestinal absorption of the acetamiprid neonicotinoid by Caco-2 cells: transepithelial transport, cellular uptake and efflux.*, J Environ Sci Health B. [1]

Dalvie D, D. (2019), “Aldehyde oxidase and its role as a drug metabolizing enzyme.”, *Pharmacol Ther.*, Vol. 201, pp. 137-80. [12]

Darwich AS, N. (2010), “Interplay of metabolism and transport in determining oral drug absorption and gut wall metabolism: a simulation assessment using the “Advanced Dissolution, Absorption, Metabolism (ADAM)” model.”, *Curr Drug Metab*, Vol. 11(9), pp. 716-29. [21]

David Dahlgren, C. (2016), “Regional Intestinal Permeability of Three Model Drugs in Human,”, PMID 27504798. [41]

Dick RA, K. (2005), “Identification of aldehyde oxidase as the neonicotinoid nitroreductase.”, *Chem Res Toxicol.*, Vol. 18(2), pp. 317-23. [6]

E A Taylor, P. (1981), “The distribution of propranolol, pindolol and atenolol between human erythrocytes and plasma,”, *Br J Clin Pharmacol*, PMID: 7295488, p. p543. [42]

Fisher C, Gardner I, Masoud J. VIVD (2017), “A virtual in vitro distribution model for predicting intra- and sub-cellular concentrations in toxicity assays.”, *Toxicology Letters*, Vol. 280(Supplement 1), p. S290. [52]

Ford KA, C. (2006), *Chloropyridinyl neonicotinoid insecticides: diverse molecular substituents contribute to facile metabolism in mice*, Chem Res Toxicol. [2]

Gao H, S. (2010), “Assessment of in silico models for fraction of unbound drug in human liver microsomes.”, *Expert Opin Drug Metab Toxicol.*, Vol. 6(5), pp. 533-42. [35]

Gertz M, H. (2010), "Prediction of human intestinal first-pass metabolism of 25 CYP3A substrates from in vitro clearance and permeability data.", *Drug Metab Dispos.*, Vol. 38(7), pp. 1147-58. [37]

Giuliano C, J. (2005), "Direct determination of unbound intrinsic drug clearance in the microsomal stability assay.", *Drug Metab Dispos.*, Vol. 33(9), pp. 1319-24. [32]

H E Barber, G. (1978), "Protein binding of atenolol and propranolol to human serum albumin and in human plasma [proceedings],", *Br J Clin Pharmacol*, PMID: 728297, p. 446P. [43]

H J Burt, S. (2016), "Metformin and cimetidine: Physiologically based pharmacokinetic modelling to investigate transporter mediated drug-drug interactions,", *Eur J Pharm Sci,*, PMID: 27019345, pp. 88:70-82. [44]

Harada KH, T. (2016), *Biological Monitoring of Human Exposure to Neonicotinoids Using Urine Samples, and Neonicotinoid Excretion Kinetics.*, PLoS One. [4]

Harwood MD, N. (2016), "Breast Cancer Resistance Protein Abundance, but Not mRNA Expression, Correlates With Estrone-3-Sulfate Transport in Caco-2.", *J Pharm Sci.*, Vol. 105(4), pp. 1370-5. [20]

Harwood MD, N. (2013), "Absolute abundance and function of intestinal drug transporters: a prerequisite for fully mechanistic in vitro-in vivo extrapolation of oral drug absorption.", *Biopharm Drug Dispos.*, Vol. 34(1), pp. 2-28. [19]

Honda H, T. (2006), "Neo-nicotinoid metabolic activation and inactivation established with coupled nicotinic receptor-CYP3A4 and -aldehyde oxidase systems.", *Toxicol Lett*, Vol. 161(2), pp. 108-14. [11]

Hosea NA, C. (2009), "Prediction of human pharmacokinetics from preclinical information: comparative accuracy of quantitative prediction approaches.", *J Clin Pharmacol.*, Vol. 49(5), pp. 513-33. [38]

Hsieh YL, I. (2012), "pH-Induced precipitation behavior of weakly basic compounds: determination of extent and duration of supersaturation using potentiometric titration and correlation to solid state properties.", *Pharm Res.*, Vol. 29(10), pp. 2738-53. [27]

Jamei M, D. (2009), "A framework for assessing inter-individual variability in pharmacokinetics using virtual human populations and integrating general knowledge of physical chemistry, biology, anatomy, physiology and genetics: A tale of 'bottom-up' vs 'top-down' recognition", *Drug Metab Pharmacokinet.*, Vol. 24(1), pp. 53-75. [14]

Jamei M, M. (2013), "The simcyp population based simulator: architecture, implementation, and quality assurance.", *In Silico Pharmacol*, Vol. 1, p. 9. [13]

Jamei M, T. (2009), "Population-based mechanistic prediction of oral drug absorption.", *AAPS J*, Vol. 11(2), pp. 225-37. [16]

Johnson TN, B. (2018), "Development and applications of a physiologically-based model of paediatric oral drug absorption.", *Eur J Pharm Sci.*, Vol. 115, pp. 57-67. [39]

Kapoor U, S. (2014), *Disposition and acute toxicity of imidacloprid in female rats after single exposure.*, Food Chem Toxicol. [5]

Kilford PJ, G. (2008), “Hepatocellular binding of drugs: correction for unbound fraction in hepatocyte incubations using microsomal binding or drug lipophilicity data.”, *Drug Metab Dispos.*, Vol. 36(7), pp. 1194-7. [31]

Kolanczyk RC, T. (2020), “In vitro metabolism of imidacloprid and acetamiprid in rainbow trout and rat.”, *Xenobiotica.*, Vol. 50(7), pp. 805-14. [7]

K, S. (2009), “Theoretical investigation of passive intestinal membrane permeability using Monte Carlo method to generate drug-like molecule population.”, *Int J Pharm.*, Vol. 373(1-2), pp. 55-61. [25]

LM., B. (2004), “Volume of distribution at steady state for a linear pharmacokinetic system with peripheral elimination.”, *J Pharm Sci*, Vol. 93(6), pp. 1628-40. [48]

McGinnity DF, B. (2006), “Evaluation of time-dependent cytochrome P450 inhibition using cultured human hepatocytes.”, *Drug Metab Dispos*, Vol. 34(8), pp. 1291-300. [30]

Musther H, H. (2017), “The Constraints, Construction, and Verification of a Strain-Specific Physiologically Based Pharmacokinetic Rat Model.”, *J Pharm Sci.*, Vol. 106(9), pp. 2826-38. [40]

Nilsson D, F. (1994), “The influence of net water absorption on the permeability of antipyrine and levodopa in the human jejunum.”, *Pharm Re*, Vol. 11(11), pp. 1540-7. [22]

Oliver RE, J. (1998), “What surface of the intestinal epithelium is effectively available to permeating drugs?”, *J Pharm Sci.*, Vol. 87(5), pp. 634-9. [26]

Poulin and Theil. (2002), “Prediction of pharmacokinetics prior to in vivo studies. 1. Mechanism-based prediction of volume of distribution.”, *J Pharm Sci.*, Vol. 91(1), pp. 129-56. [51]

Rodgers and Rowland (2006), “Physiologically based pharmacokinetic modelling 2: predicting the tissue distribution of acids, very weak bases, neutrals and zwitterions.”, *J Pharm Sci.*, Vol. 95(6), pp. 1238-57. [50]

S H Wan, R. (1979), “Pharmacokinetics, pharmacology of atenolol and effect of renal disease,”, *Br J Clin Pharmacol*, PMID: 465278, p. p 569. [47]

Sawada Y, H. (1984), “Prediction of the volumes of distribution of basic drugs in humans based on data from animals.”, *J Pharmacokinet Biopharm.*, Vol. 12(6), pp. 587-96. [15]

Schulz-Jander DA, C. (2002), “Imidacloprid insecticide metabolism: human cytochrome P450 isozymes differ in selectivity for imidazolidine oxidation versus nitroimine reduction.”, *Toxicol Lett*, Vol. 132(1), pp. 65-70. [8]

Schulz-Jander DA, L. (2002), “Neonicotinoid insecticides: reduction and cleavage of imidacloprid nitroimine substituent by liver microsomal and cytosolic enzymes.”, *Chem Res Toxicol*, Vol. 15(9), pp. 1158-65. [9]

Sun D, L. (2002), “Comparison of human duodenum and Caco-2 gene expression profiles for 12,000 gene sequences tags and correlation with permeability of 26 drugs.”, *Pharm Res.*, Vol. 19(10), pp. 1400-16. [23]

Terayama H, E. (2016), *Acetamiprid Accumulates in Different Amounts in Murine Brain Regions.*, Int J Environ Res Public Health. [3]

Turner DB, R. (2006), “Prediction of non-specific microsomal binding from readily available physicochemical properties.”, *9th European ISSX meeting, Manchester, UK.*. [34]

W D Mason, N. (1979), “Kinetics and absolute bioavailability of atenolol, Clin Pharmacol Ther.,”, PMID: 428185, p. p408. [46]

W Kirch, H. (1981), “Pharmacokinetics of atenolol in relation to renal function, Kinetics and absolute bioavailability of atenolol,”, *Eur J Clin Pharmacol,*, PMID: 7461026, p. 19p. [45]

Wang J, F. (2002), “General solution for diffusion-controlled dissolution of spherical particles. 2. Evaluation of experimental data.”, *J Pharm Sci*, Vol. 91(2), pp. 534-42. [18]

Wang J, F. (1999), “General solution for diffusion-controlled dissolution of spherical particles. 1. Theory.”, *J Pharm Sci.*, Vol. 88(7), pp. 731-8. [17]

Wang X, A. (2018), “Mechanism of Neonicotinoid Toxicity: Impact on Oxidative Stress and Metabolism.”, *Annu Rev Pharmacol Toxicol.*, Vol. 58, pp. 471-507. [10]

Winiwarter S, B. (1998), “Correlation of human jejunal permeability (in vivo) of drugs with experimentally and theoretically derived parameters. A multivariate data analysis approach.”, *J Med Chem.*, Vol. 41(25), pp. 4939-49. [24]

Yang J, J. (2007), “Prediction of intestinal first-pass drug metabolism.”, *Curr Drug Metab*, Vol. 8(7), pp. 676-84. [36]

Zhang Y, Y. (2010), “Lack of appreciable species differences in nonspecific microsomal binding.”, *J Pharm Sci.*, Vol. 99(8), pp. 3620-7. [33]